The impact of Aeolus winds on near-surface wind forecasts over tropical ocean and high-latitude regions

Haichen Zuo[1], Charlotte Bay Hasager[1]

[1]Wind and Energy Systems, Technical University of Denmark, Roskilde, 4000, Denmark

Correspondence to: Haichen Zuo (hazu@dtu.dk)

Abstract. To detect global wind profiles and improve numerical weather prediction (NWP), the European Space Agency (ESA) launched the Aeolus satellite carrying a space-borne Doppler Wind Lidar in 2018. After the successful launch, the European Centre for Medium-Range Weather Forecasts (ECMWF) performed the observing system experiments (OSEs) to evaluate the contribution of Aeolus data to NWP. This study aims to assess the impact of Aeolus wind assimilation in the ECMWF model on near-surface (10 m height) wind forecasts over tropical ocean regions by taking buoy measurements for reference and over high-latitude regions by taking weather station data for reference for the year 2020. The assessments were conducted through inter-comparison analysis and triple collocation (TC) analysis. The results of the inter-comparison analysis show that Aeolus data assimilation has a limited impact on sea surface wind forecasts for tropical regions when compared with buoy measurements. For the high-latitude regions in the Northern Hemisphere, Aeolus has the potential to improve near-surface wind forecasts. This positive impact is more evident as the forecast time step extends, during the first half-year of 2020, and during the winter months. In addition, the v component tends to benefit more from the Aeolus observations than the u component. For the Southern Hemisphere, a few error reductions are observed but exist randomly. The research findings from TC are consistent with the results of inter-comparison analyses for most cases. Overall, this in situ data-based assessment expands our understanding of the role of Aeolus data assimilation with the global NWP model in predicting near-surface wind for tropical oceans and high-latitude regions.

1 Introduction

For characterizing global wind profiles and improving numerical weather prediction (NWP), the first space-borne Doppler Wind Lidar (DWL) carried by the Aeolus satellite was launched in August 2018 by the European Space Agency (ESA). The mission is still ongoing and has been operating for more than four years. Following a sun-synchronous orbit, Aeolus passes over the equator at 06:00 local time (LT) during descending orbits and 18:00 LT during ascending orbits and samples the whole globe every twelve hours with eight orbits. Wind retrieval of Aeolus is based on the Doppler shifted frequency between emitted light pulses and backscattered light from air molecules (i.e. Rayleigh scattering) as well as from large particles, such as cloud droplets and ice crystals, in the atmosphere (i.e. Mie scattering). By measuring this small difference, wind velocity along the line-of-sight (LOS) can be obtained, which is further converted to the approximately east-west

horizontal LOS wind component using the off-nadir angle of 35° (Andersson et al., 2008). The detected wind profiles, ranging from the surface to about 30 km in height with 24 vertical bins, can be used to improve NWP, capture gravity waves, track volcanic eruptions, etc. (Banyard et al., 2021; Rennie et al., 2021; Parrington et al., 2022).

After the successful launch, calibration and validation works have been widely carried out worldwide. Owing to the continually improved data processing chain, from Baseline 10 with M1-temperature-based bias correction and daily updates of global offset bias removal (Data Innovation and Science Cluster, 2020), the systematic errors of both Rayleigh-clear winds and Mie-cloudy winds are almost within 0.5 m s^{-1} despite some cases in the polar regions, and the random errors mainly vary between 4 m s^{-1} and 8 m s^{-1} for Rayleigh-clear winds and between 2.0 m s^{-1} and 5 m s^{-1} for Mie-cloudy winds (Belova et al., 2021; Iwai et al., 2021; Witschas et al., 2022; Zuo et al., 2022). However, what should be noted is that Aeolus has been suffering unexpected signal loss since the launch, probably due to the decreasing emitted laser energy for the FM-A period (August 2018 – June 2019) and/or laser-induced contamination for the FM-B period (July 2019 – September 2022) (Straume-Lindner et al., 2021). The data quality assessment based on the second reprocessed data set (2B11) by the European Centre for Medium-Range Weather Forecasts (ECMWF) revealed that the estimated random error of Rayleigh-clear wind increased by 40% from ~5 m s^{-1} to ~7 m s^{-1} during July 2019 – October 2020 due to the gradual signal reduction of DWL, while this instrument issue has less influence on Mie-cloudy winds with estimated random errors remaining at ~3.5 m s^{-1} (Rennie and Isaksen, 2022).

Although Aeolus suffers from unexpected signal loss and growing errors, its wind products have been employed to improve NWP through data assimilation, an approach that integrates recent observations with a previous forecast to achieve the best estimate of the current atmospheric state (ECMWF, 2020). For evaluating the contribution of Aeolus observations to NWP, the observing system experiments (OSEs) with and without Aeolus data assimilation have been performed with global NWP models at many institutions, including the ECMWF, National Oceanic and Atmospheric Administration (NOAA), Deutscher Wetterdienst (DWD), Météo-France, UK Met Office, etc. (Cress et al., 2022; Garrett et al., 2022; Forsythe and Halloran, 2022; Pourret et al., 2022; Rennie and Isaksen, 2022). The assessment of the ECMWF OSEs demonstrated that Aeolus winds are able to improve wind vector and temperature forecasts, especially in the upper troposphere and/or lower stratosphere over tropical and polar regions (Rennie et al., 2021). Similar results were also found from the OSEs with NOAA's Global Forecast System, the DWD model and the Environment and Climate Change Canada global forecast system (Cress et al., 2022; Garrett et al., 2022; Laroche and St-James, 2022). Moreover, regarding the weather and climate events, Aeolus is able to improve the track forecasts for tropical cyclones in the Eastern Pacific basin and Atlantic basin (Garrett et al., 2022) and benefits the forecasts of the West African Monsoon as well as the changes in the El Niño-Southern Oscillation (ENSO) state over the Eastern Pacific by capturing the large-scale atmospheric circulation (Cress et al., 2022). However, the existing assessments mainly focused on the forecasts at pressure levels or upper air, while the impacts of Aeolus data assimilation on near-surface wind forecasts lack detailed study. This research gap needs to be complemented since the relevant scientific

investigation could provide valuable information for future applications in wind-related activities, such as ocean shipping and wind farm operation and maintenance. Due to the relatively low spatial and temporal resolution of Aeolus wind observations, global models are more likely to benefit from Aeolus data assimilation than high-resolution regional models (Hagelin et al., 2021; Mile et al., 2022; Rennie and Isaksen, 2022). Therefore, as a starting point, we would like to focus on the ECMWF model first. This will give us a better understanding of the influence of Aeolus on near-surface wind forecasts, which in turn guides us to apply Aeolus winds to regional models for practical applications. Considering tropical oceans and polar regions are favourable to extreme weather but lack in situ measurements and the model performance is usually not satisfactory in these regions, such as large bias over Inter-Tropical Convergence Zone (ITCZ) (Sandu et al., 2020), we would like to investigate whether the Aeolus can contribute to more reliable wind forecasts for these regions.

Regarding the reference data set for evaluation, many verifications related to Aeolus OSEs were conducted by inter-comparing with model analysis that has global coverage and deals with the representation error between model scale and scales of observations (Garrett et al., 2022; Pourret et al., 2022; Rennie and Isaksen, 2022). However, there are fewer in situ measurements available over tropical and polar regions, and the mesoscale convections are not resolved well in the global NWP models, which leads to the large uncertainties of model analysis data in these regions (Sandu et al., 2020; King et al., 2022). Given this, taking in situ measurements as the reference can avoid this issue to some extent.

In terms of the evaluation method, apart from the conventional inter-comparison analysis, triple collocation (TC) analysis is another beneficial method for environmental parameter evaluation when there are three independent data sets (Stoffelen, 1998; Vogelzang and Stoffelen, 2012). Different from the inter-comparison analysis that regards a reference data set free of errors, TC analysis assumes that each system is linearly correlated with the truth. Furthermore, TC analysis takes representation errors into account when three data sets have different spatial and temporal resolutions, and the result is with respect to the medium or lowest resolution among three systems. The primary outputs of TC include the error standard deviation (or random error) of each system and calibration coefficients based on a reference data set (Vogelzang and Stoffelen, 2012). TC method has been widely implemented to characterize the errors for wind measurements from scatterometers, altimeters, and DWL, etc. (Caires and Sterl, 2003; Vogelzang et al., 2011; Ribal and Young, 2020; Cossu et al., 2022). However, to the author's best knowledge, no studies have evaluated wind forecasts by this method so far.

Hence, to complement the existing studies, this study aims to assess the impact of Aeolus wind assimilation on near-surface wind forecasts over tropical ocean regions between 30° N and 30° S by taking buoy measurements for reference. Furthermore, we investigated the high-latitude region > 60 °N in the Northern Hemisphere (NH) and the high-latitude region > 60° S in the Southern Hemisphere (SH) by taking weather station data for reference. Our hypothesis is that the assimilation of Aeolus winds will reduce the forecast error. Since the overall data quality of Aeolus is reduced in the second half-year of 2020 compared to the first half-year due to the weakening signals, our hypothesis is that the assimilation of Aeolus winds

can reduce the forecast error relatively more during the first half-year compared to the second half-year. In the tropics, seasonal effects are very limited, while in the high-latitude regions, the seasonal variability is high, so for those we also investigated the forecast for the seasons, mainly for the summer and winter months of each hemisphere. The assessments were conducted mainly through inter-comparison analysis based on a high-resolution $T_{co}639$ OSE in the ECMWF model for the entire year of 2020. Additionally, we attempted to quantify and compare the random errors of the two forecasts by using the triple collocation method.

Section 2 and Sect. 3 introduce the data and methods used in this study. Sect. 4 presents the main research findings, followed by Sect. 5 for discussions. The final Sect. makes a short summary of the study and draws conclusions.

2 Data

2.1 Observing System Experiments with ECMWF model

This study is based on the ECMWF OSEs with the 2nd reprocessed Aeolus L2B baseline 11 data assimilated during the FM-B period (Rennie and Isaksen, 2022). The applied model version is CY47R2 with an atmosphere outer loop resolution of T_{co} 639 L137 (~ 18 km grid). Observations from nominally operational satellites and conventional sources were assimilated. The OSEs include a control experiment without Aeolus assimilation and an experiment with Aeolus Rayleigh-clear and Mie-cloudy wind assimilation through the four-dimensional variational (4D-Var) data assimilation technique. For the lower troposphere (> 850 hPa), only Mie-cloudy winds with an estimated error smaller than 5 m s^{-1} were assimilated into the model. Detailed information on quality control decisions for the OSEs is documented in Rennie and Isaksen (2022). Figure 1 illustrates the geographical distribution of the averaged number of L2B Mie-cloudy winds assimilated per cycle below 850 hPa. More low-level Aeolus winds are assimilated over the ocean regions than inland regions and over low-to-mid-latitude regions than high-latitude regions.

Wind forecast errors from the two OSEs are considered uncorrelated because as the forecast extends, the different initial conditions may lead to the random errors being more independent. Thus, to carry out TC analysis and simplify the equations, we assume that the errors from the two model runs are independent over the whole forecast range.

The 10-day forecasts based on the 00 UTC analysis of zonal (u) and meridional (v) wind components at 10 m height were obtained from the ECMWF Meteorological Archival and Retrieval System (MARS) for evaluation (ECMWF Research Department, 2022). The interval of forecast steps is 24 hours. The data cover the completed year of 2020.

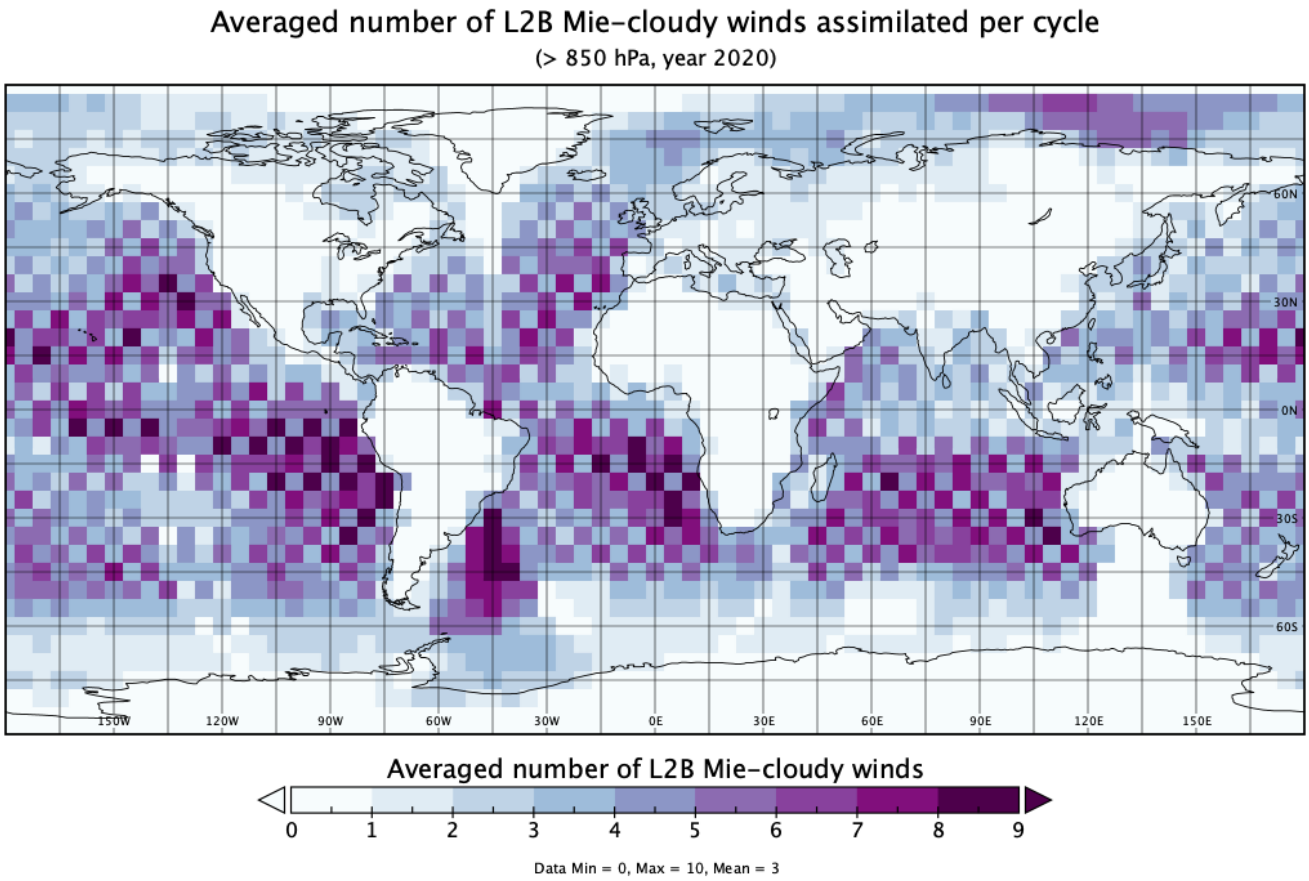

Figure 1: Map of the averaged number of L2B Mie-cloudy winds at pressure > 850 hPa assimilated into the model

2.2 Buoy measurements

The tropical moored buoy measurements over the Atlantic Ocean, Indian Ocean and Pacific Ocean were obtained from Global Tropical Moored Buoy Array (Pacific Marine Environmental Laboratory, n.d.). The extracted parameters include zonal (u) and meridional (v) wind components, wind speed, and wind direction with a temporal resolution of 10 minutes or 1 hour. The missing value and data flagged low-quality have been removed. Finally, there are 11 buoys available in the Atlantic Ocean, 9 in the Indian Ocean and 55 in the Pacific Ocean, the locations of which are displayed in Fig. 2. To make all measurements have an identical temporal resolution, we averaged the 10 minutes wind speeds to hourly wind speeds. Furthermore, to collocate with wind forecasts from the OSEs, the buoy winds were extrapolated from its anemometer height of 3.5 m or 4 m to 10 m by using the method described in Bidlot et al. (2002).

2.3 Weather station data

Surface synoptic observations over high-latitude regions (> 60° N and > 60° S) were extracted from Global Hourly - Integrated Surface Database (ISD) (National Centers for Environmental Information, n.d.). Only the wind speeds and directions passed all quality control checks were kept for further analysis. Additionally, we calculated the correlation coefficients (R) between in situ measurements and the control experiments at T+0 h, and the stations with weak correlations (R < 0.5) were removed. One reason is that when the poor correlations are caused by very limited data samples during the study period, such as due to freeze or instrument malfunction, we consider the data quality of those available samples are still questionable. Another reason is that the weak correlations may imply the limited spatial representativeness of those stations, especially over the complex terrain. After quality control, there are 751 (223) and 56 (30) stations available (removed) over the high-latitude regions in the Northern and Southern Hemisphere, respectively (Fig. 2).

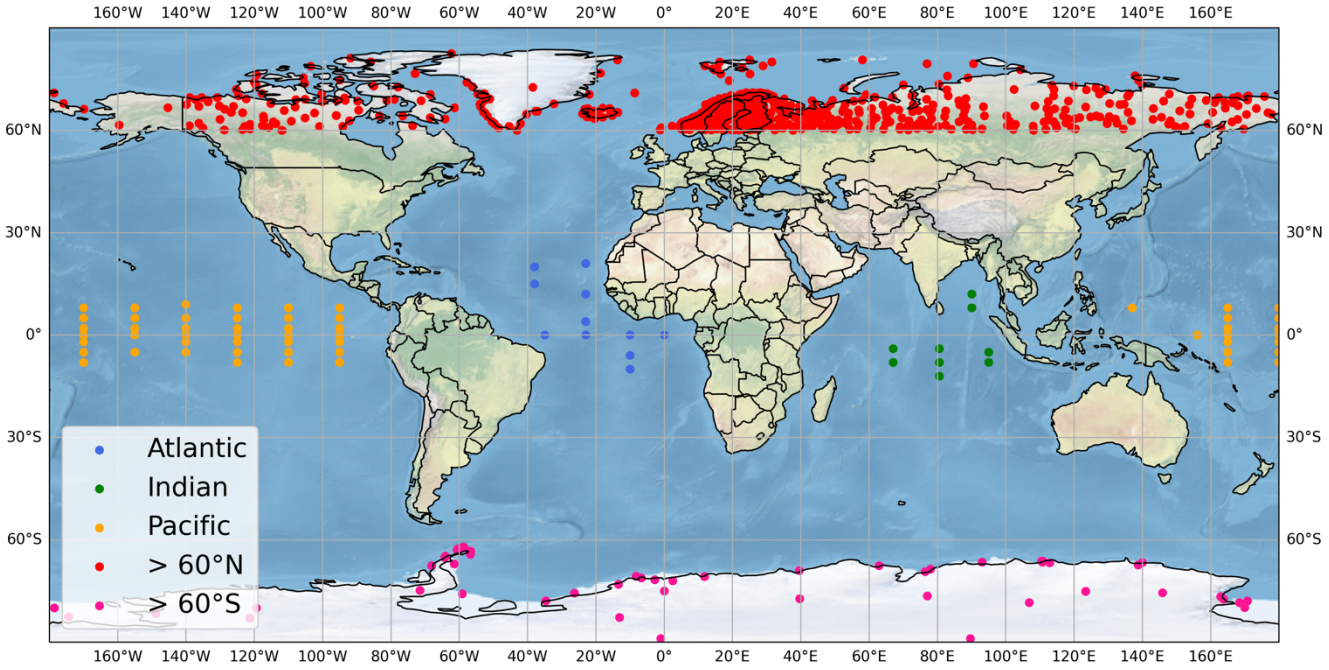

Figure 2: The geographical location of moored buoys in the tropical oceans and weather stations in the high latitude > 60° N and high latitude > 60° S (background image made with Natural Earth. Free vector and raster map data at naturalearthdata.com).

3 Method

3.1 Inter-comparison analysis

To evaluate the wind forecasts from OSEs, we take buoy measurements or weather station observations as reference, respectively. We quantified the normalized change in the root-mean-square errors (RMSE) with and without Aeolus data

assimilation for all paired data samples, thus determining whether the Aeolus can improve the model performance or not over each study region. The normalized change in RMSEs (NCRMSE) is given as

$$NCRMSE = \frac{\sqrt{\frac{\sum_{i=1}^{N}\left(f_{i,with\ Aeolus} - o_{i,in\ situ}\right)^2}{N}} - \sqrt{\frac{\sum_{i=1}^{N}\left(f_{i,no\ Aeolus} - o_{i,in\ situ}\right)^2}{N}}}{\sqrt{\frac{\sum_{i=1}^{N}\left(f_{i,no\ Aeolus} - o_{i,in\ situ}\right)^2}{N}}} \quad (1)$$

where $f_{i,with\ Aeolus/no\ Aeolus}$ is the wind forecast with or without Aeolus data assimilation; $o_{i,in\ situ}$ is the in situ measurements from either buoys or weather stations; and N is the total number of paired data samples for each study region or each case. The statistical significance of NCRMSE was quantified at the 95% confidence interval (not shown on plots).

3.2 Triple collocation analysis

In addition to inter-comparison analysis, we conducted the evaluation via triple collocation (TC) method that assumes that each system (i.e. data set) is linearly correlated with the truth at the scales commonly captured by all three systems. By taking one system as a reference (i.e. free of system error), the error standard deviation or random error of each system can be quantified (Vogelzang and Stoffelen, 2012).

In this study, we take the in situ measurements as the reference, defined as system 1. Systems 2 and 3 are the control experiment without Aeolus data assimilation and the experiment with Aeolus data assimilation, respectively. Table 1 gives the temporal and spatial resolutions of these three systems. Eq. (2), (3) and (4) describe the linear relation of each system with the true wind.

$$U_1 = t + e_1 \quad (2)$$

$$U_2 = a_2 + b_2 t + e_2 \quad (3)$$

$$U_3 = a_3 + b_3 t + e_3 \quad (4)$$

U_i is the wind component (u or v) of each system; t is the true value of a wind component; a_i and b_i are the intercept and the gradient of the calibration for each system; e_i is the true random error of each system.

Table 1. Spatial and temporal resolution of the three systems

	1: In situ	2: Experiment (No Aeolus)	3: Experiment (With Aeolus)
Horizontal	Point-based	~ 18 km grid size	~ 18 km grid size
Height	10 m	10 m	10 m
Temporal	hourly	Instantaneous	Instantaneous

Detailed information on the TC method and its related equation derivation can be found in Stoffelen (1998) and Vogelzang and Stoffelen (2012). The error variance for each system is given by the following (Ribal and Young, 2020):

$$\sigma_1^2 = \langle e_1^2 \rangle = C_{11} - \frac{(C_{12} - < e_1 e_2 >)(C_{13} - < e_1 e_3 >)}{C_{23} - < e_2 e_3 >} \quad (5)$$

$$\sigma_2^2 = \langle e_2^2 \rangle = C_{22} - \frac{(C_{12} - < e_1 e_2 >)(C_{23} - < e_2 e_3 >)}{C_{13} - < e_1 e_3 >} \quad (6)$$

$$\sigma_3^2 = \langle e_3^2 \rangle = C_{33} - \frac{(C_{23} - < e_2 e_3 >)(C_{13} - < e_1 e_3 >)}{C_{12} - < e_1 e_2 >} \quad (7)$$

where C_{ii} is the variance of each system, and C_{ij} is the covariance between the system i and j; and $\langle e_i e_j \rangle$ is the representation error of the error covariance between the system i and j.

When implementing the triple collocation method for three systems with different resolutions, such as buoy measurements (point-based), scatterometer winds (25 km) and forecast winds from a global model (effective resolution: ~150-200 km), we need to take representation error into account since the model cannot resolve the signal seen by buoys and the scatterometers (Vogelzang and Stoffelen, 2012). In our case, two model runs have the same spatial and temporal resolution, as shown in Table 1. There is no common signal of System 1 (in situ measurements) and System 2 or 3 (control experiment or experiment with Aeolus data) not resolved by System 3 or 2 (experiment with Aeolus data or control experiment), which implies the representation errors of the error covariance are zero (i.e. $< e_1 e_2 > = < e_1 e_3 > = 0$). The forecast errors from the two model runs are assumed uncorrelated, thus $< e_2 e_3 > = 0$. After simplifying the Eq. (5)-(7), the error standard deviation calculation is given in Eq. (8), (9) and (10).

$$\sigma_1 = \sqrt{\langle e_1^2 \rangle} = \sqrt{C_{11} - \frac{C_{12}\, C_{13}}{C_{23}}} \quad (8)$$

$$\sigma_2 = \sqrt{\langle e_2^2 \rangle} = \sqrt{C_{22} - \frac{C_{12} C_{23}}{C_{13}}} \quad (9)$$

$$\sigma_3 = \sqrt{\langle e_3^2 \rangle} = \sqrt{C_{33} - \frac{C_{23} C_{13}}{C_{12}}} \quad (10)$$

where $\frac{C_{12}\, C_{13}}{C_{23}}$ is the common true variance, denoted as CTV in the plots hereafter. The statistical significance of error standard deviations for wind forecasts was quantified at the 95% confidence interval by using the bootstrap method. The TC results enable us to compare the random error of each system directly, with σ_3 smaller than σ_2 implying positive impact of Aeolus, which is equivalent to the negative NCRMSE if using the inter-comparison analysis.

The analyses were performed for each ocean basin, regions > 60° N and > 60° S, respectively, aiming to provide error information geographically. We focus on error information of each wind component as well as wind speed instead of vector wind as the former is more relevant to practical applications. We also divided the study period into two half-years to evaluate the sensitivity of Aeolus data quality on wind forecast. For high-latitude regions, the study was also carried out for each

season. Since the error model of TC works better for noisy u and v wind components than wind speed (Stoffelen, 1998), the triple collocation analyses were only performed for wind components. In addition, TC analyses were carried out based on all collocated data samples over each study region rather than from each site since the optimal number of data samples for TC is at least 1000. To be consistent with TC, inter-comparison analyses were also performed based on all paired data samples. Moreover, for the region > 60° N, we divided the data samples into four categories based on the in situ wind speeds (Table 2) and investigated the impact of Aeolus under different wind speed ranges (Met Office, 2023). Apart from these, the Pearson correlation coefficient of each two systems was also calculated as the additional statistical information to facilitate the study.

Table 2. Wind speed categories.

Category	Wind speed range [m s^{-1}]	Description
a	wspd ≤ 6.0	Light air to gentle breeze
b	6.0 < wspd ≤11.0	Moderate breeze to fresh breeze
c	11.0 < wspd ≤17.0	Strong breeze to near gale
d	wspd > 17.0	Gale to hurricane

4 Results

4.1 Tropical oceans

4.1.1 Inter-comparison analysis

Figure 3 shows the NCRMSEs from inter-comparison analyses for three ocean basins. For the tropical Atlantic Ocean, the negative values are mainly found within T+72 h for the v vector and wind speed. The results for the tropical Indian Ocean do not show any trend in error reduction for wind components and wind speed. Compared to the tropical Atlantic Ocean and Indian Ocean, the Pacific witnesses negative values at more forecast steps, but the magnitude is weaker mainly within 1%. The negative values at T+48 h for both wind components and wind speed are common for the three ocean basins. Unfortunately, all the negative NCRMSEs are not statistically significant at the 95% confidence interval; thus, the overall impact of Aeolus on sea surface wind forecast is neutral for tropical regions. According to the results for two half-years (Fig.4), Aeolus data quality seems to have no influence on improving surface wind forecasts over the tropical ocean regions.

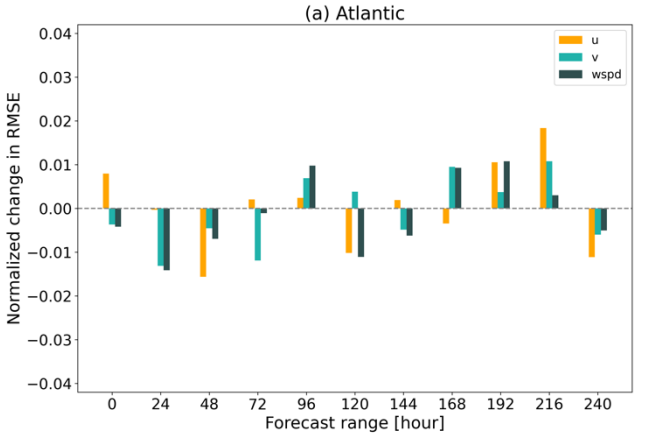

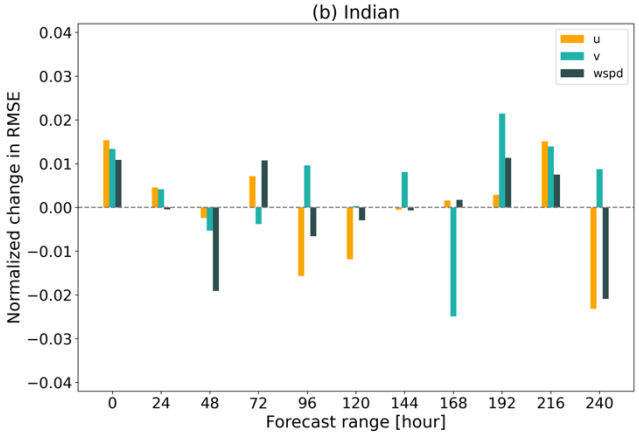

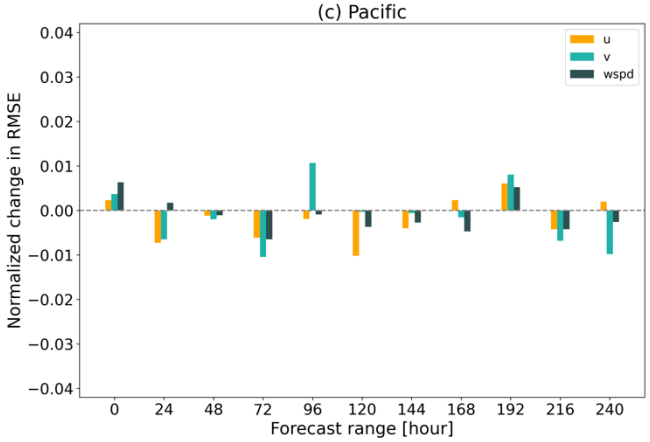

230

Figure 3: Normalized change in RMSE for u, v wind components and wind speed (wspd) for the tropical Atlantic Ocean (a), Indian Ocean (b) and Pacific Ocean (c) for the year 2020 based on ECMWF OSE forecasts with and without Aeolus against buoy data. Note that negative values indicate error reduction, implying the improvement in the forecast with Aeolus assimilation.

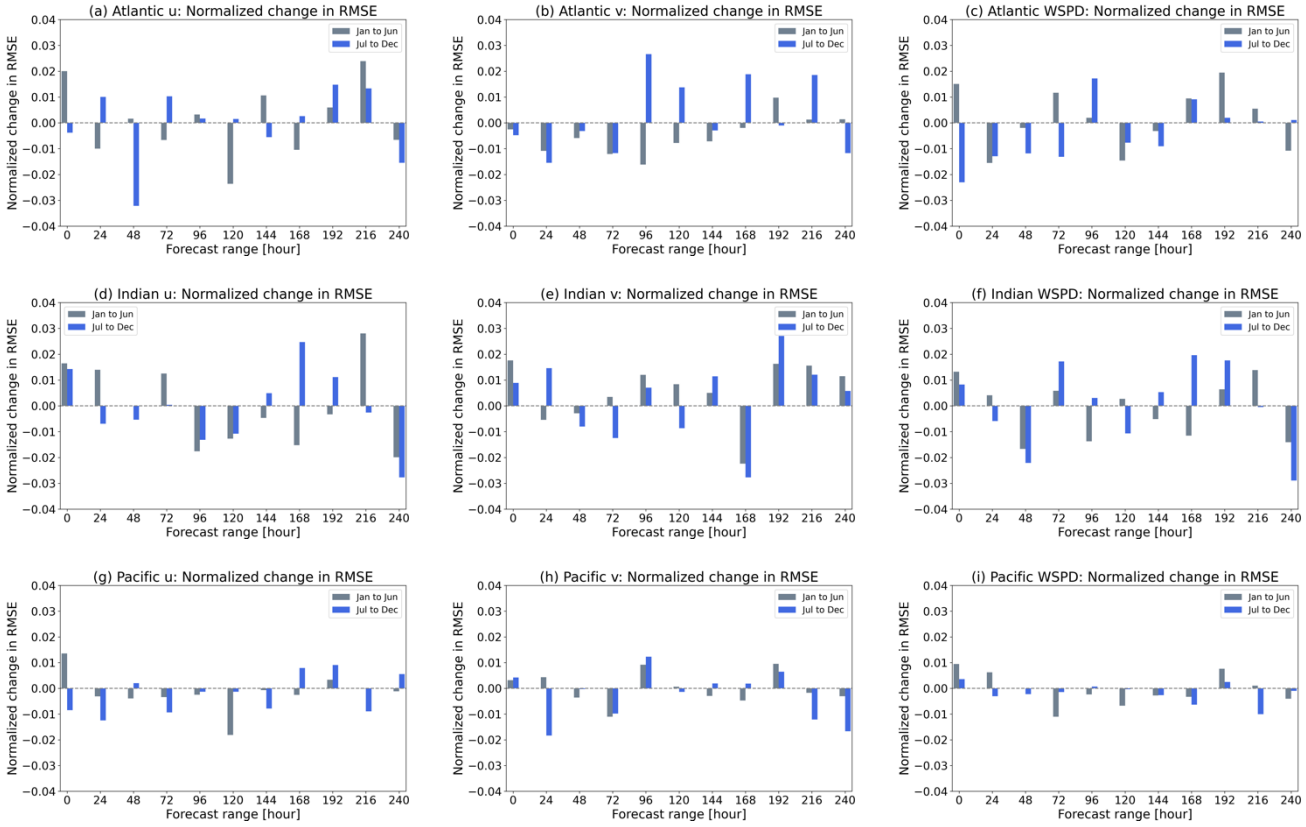

Figure 4: Normalized change in RMSE for u, v wind components and wind speed (wspd) during the first and the second half-year of 2020 for the tropical Atlantic Ocean (a, b and c), Indian Ocean (d, e and f) and Pacific Ocean (g, h and i) based on the ECMWF OSE forecasts with and without Aeolus data assimilation.

4.1.2 Triple collocation analysis

The results from the triple collocation analysis for each ocean basin are shown in Figure 5. With the forecast time extending, the error standard deviations of the OSEs and buoys increase slightly for both u and v components, and the common true variances decrease gradually with forecast time for all cases. The error standard deviations are mainly within 1 m s^{-1} from the two experiments, which are much lower than the buoy errors (> 1 m s^{-1}) for all three ocean basins since the true value of TC analysis is specified at the coarsest resolution among the three systems that is the model resolution in this study. The OSEs have an effective resolution of ~144 km (about 8 times the grid size) (Abdalla et al., 2013), which allows the model to capture large-scale atmospheric signals while small-scale details are lost. Consequently, errors from the two OSEs are smaller. Larger random errors of buoys are primarily due to the temporal and spatial representation errors related to collocation and the coarse model effective resolution. Based on the results in Fig. 5, the impacts of Aeolus data assimilation on the forecasts for the tropical ocean basins are nearly neutral. In terms of the results for two half-year periods, there are no evident differences in error characteristics between the first and second half-year of 2020 for each ocean basin (Fig.6 and Appendix A).

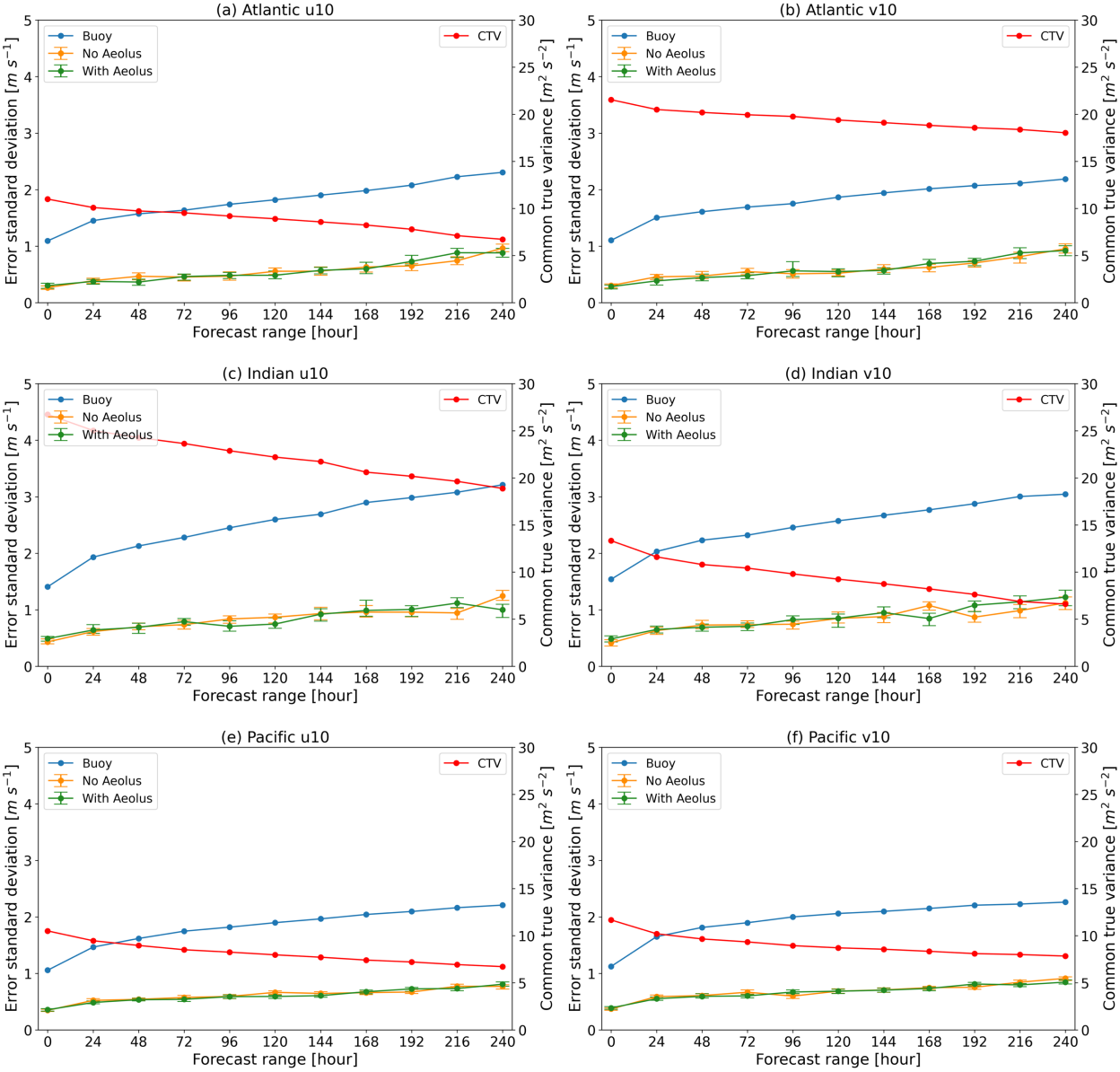

255

Figure 5: Error standard deviation and common true variance (CTV) of u and v wind components from triple collocation for the tropical Atlantic Ocean (a and b), Indian Ocean (c and d) and Pacific Ocean (e and f) for the year of 2020 based on the ECMWF OSE forecasts with and without Aeolus data assimilation and buoy data.

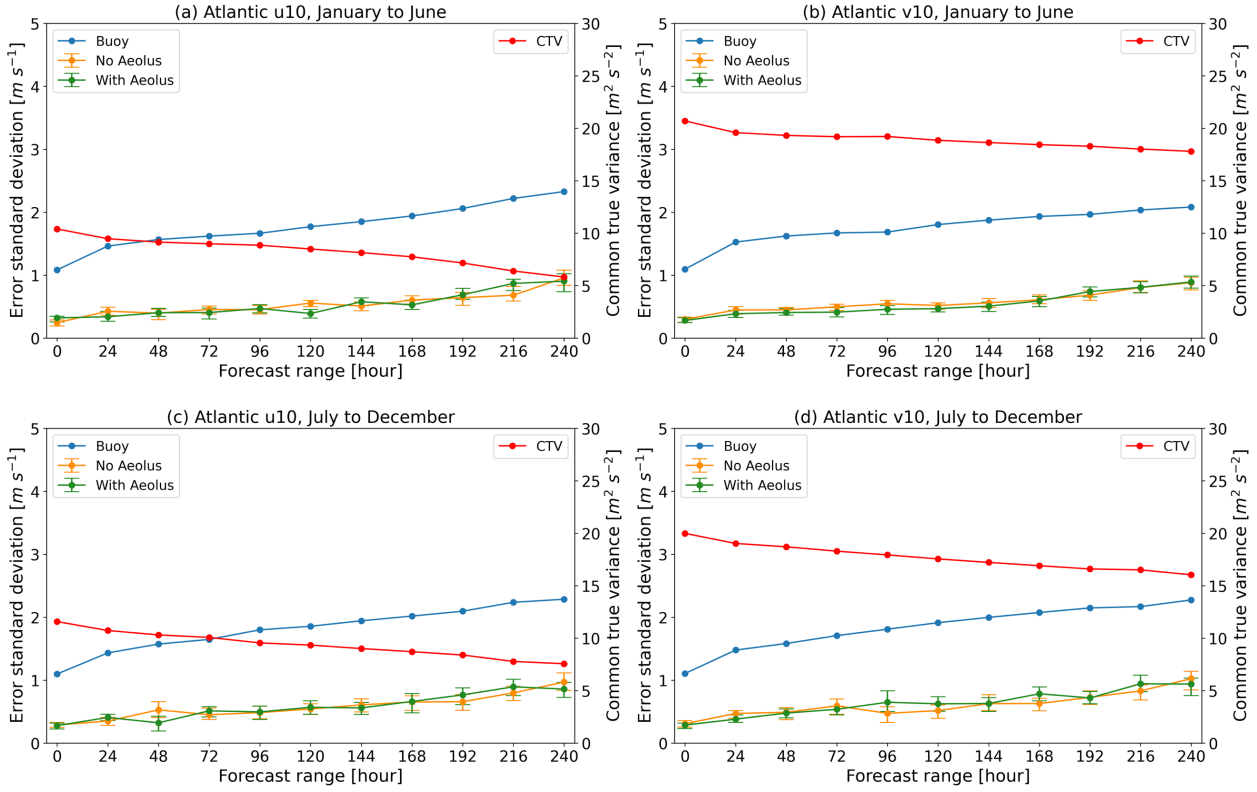

Figure 6: Same as Fig. 4 but for the first (a and b) and the second half-year (c and d) of 2020 over the tropical Atlantic Ocean.

4.1.3 Correlations of datasets

The correlation coefficients show that the forecast experiment with and without Aeolus is highly correlated up to T+120 h, with R-values greater than 0.9 for both u and v components as well as wind speed. As the forecast extends, the correlations between each two systems weaken but do not decrease too much for tropical ocean basins with R-values greater than 0.7 at T+240 h for most cases. Figure 7 is an example for the tropical Pacific at T+120 h forecast step. The results show the u and v components with R-values around 0.95 for the forecasts with and without Aeolus, while for wind speed, R-value is around 0.90. The R-values for the u component are around 0.81 for the forecasts (with/without Aeolus data) versus buoy data (Fig. 7 (e) and (f)), and for the v component the R-values are about 0.80 (Fig. 7 (h) and (i)), which indicates there is almost no increase in correlation after assimilating Aeolus winds. In summary, the zonal and meridional wind components are better resolved in the forecast model than the wind speed. The correlations do not reveal much improvement in forecast skill between the two forecasts. Similar results are found for the tropical Atlantic Ocean and Indian Ocean (not shown).

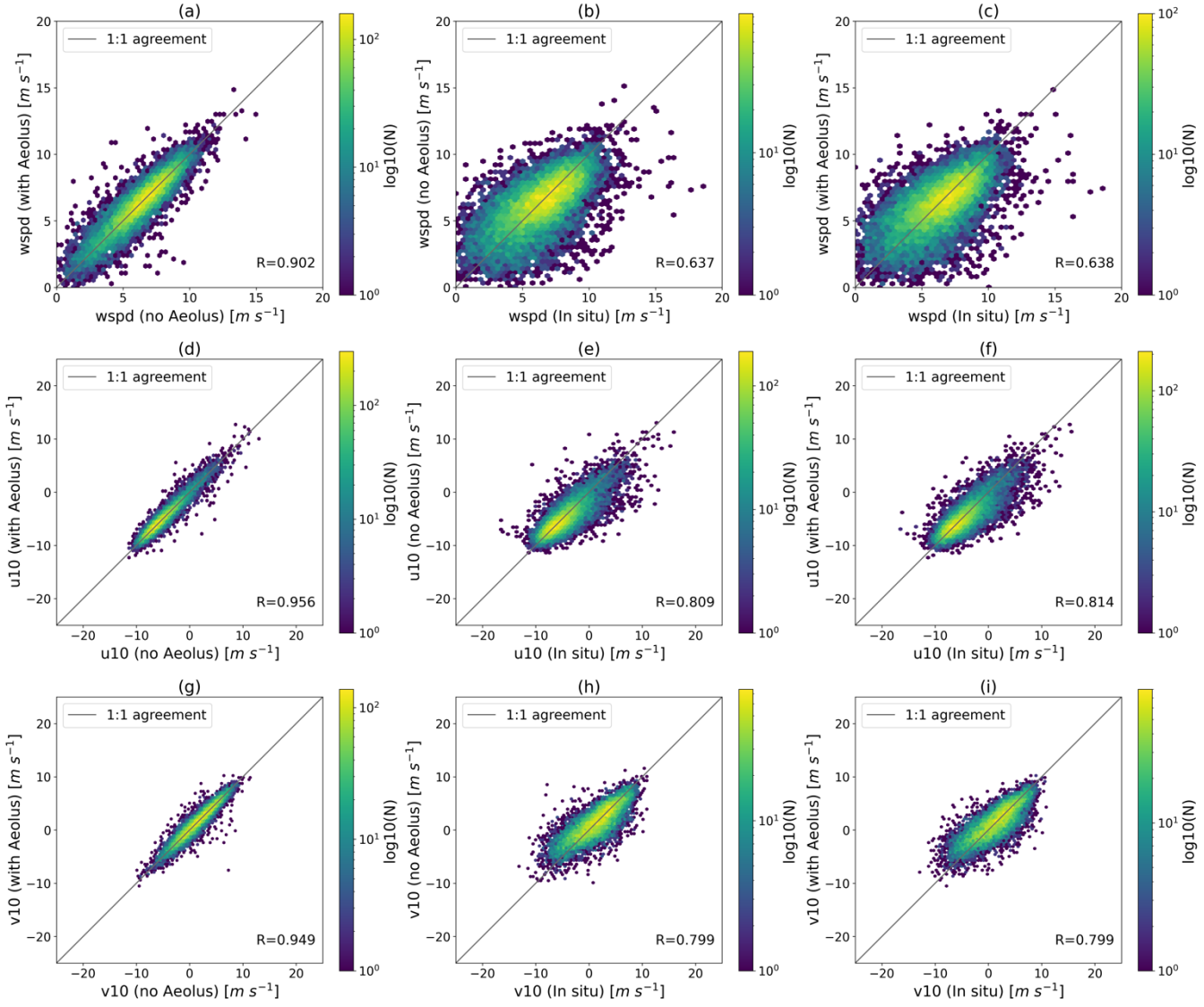

Figure 7: Hexagonal binning plots of u, v components and wind speed (wspd) at T+120 hour forecast for the tropical Pacific Ocean for the year 2020 based on ECMWF OSE forecasts with and without Aeolus and buoy data. The colour of each hexagon indicates the number of samples in it.

4.2 High-latitude region in the Northern Hemisphere (> 60° N)

4.2.1 Inter-comparison analysis

Over the high-latitude region in Northern Hemisphere, the NCRMSEs for u, v components and wind speed are almost negative and decrease as the forecast time extends, which implies Aeolus tends to make a positive contribution to medium-range near-surface wind forecast (Fig. 8). The significant positive impact is found at T+120 h, +216 h and 240 h for the u component, from T+192 h for the v component, and at T+192 h and T+216 h for wind speed. More positive impact of Aeolus was found on the v component, with the largest error reduction of 2.4% at T+216 h. Regarding the results for different wind speed categories (Fig.9), the noticeable error reductions tend to exist earlier from T+96 h forecast step for moderate to fresh breeze ($6 < \text{wspd} \leq 11$ m s^{-1}) compared to the light wind category; for the category of strong breeze to near gale ($11 < \text{wspd} \leq 17$ m s^{-1}), the negative NCRMSEs for v component exist from the T+120 h forecast step; while the largest impact on u and v components are observed at T+216 h and T+192 h, respectively, when wind speeds greater than 17 m s^{-1}, but a further demonstration is required due to limited amount of data samples in this category (N: around 1200). In terms of the results for two half-years, the NCRMSEs of u and v components are lower since T+120 h during the first half-year compared with those for the second half-year (Fig.10 (a) and (b)). This suggests that Aeolus's data quality is important for near-surface wind forecasts. With respect to the results for each season (Fig.11), Aeolus makes more contribution from T+120 h onwards to the u component forecasts during boreal winter (January, February and December) than during the boreal summer (June, July and August). For the v component, the most noticeable error reductions of 3.3% exist at T+168 h during winter months and 4.4% at T+216 h during spring (March, April and May).

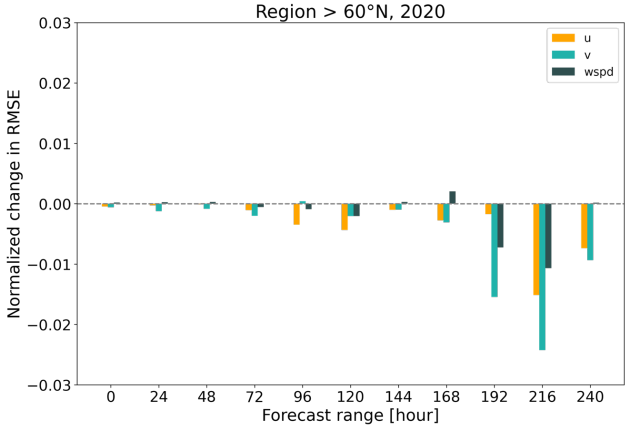

Figure 8: Normalized change in RMSE of u, v components and wind speed (wspd) as a function of forecast range for the region > 60° N for the year 2020 based on the ECMWF OSE forecasts with and without Aeolus and weather station data.

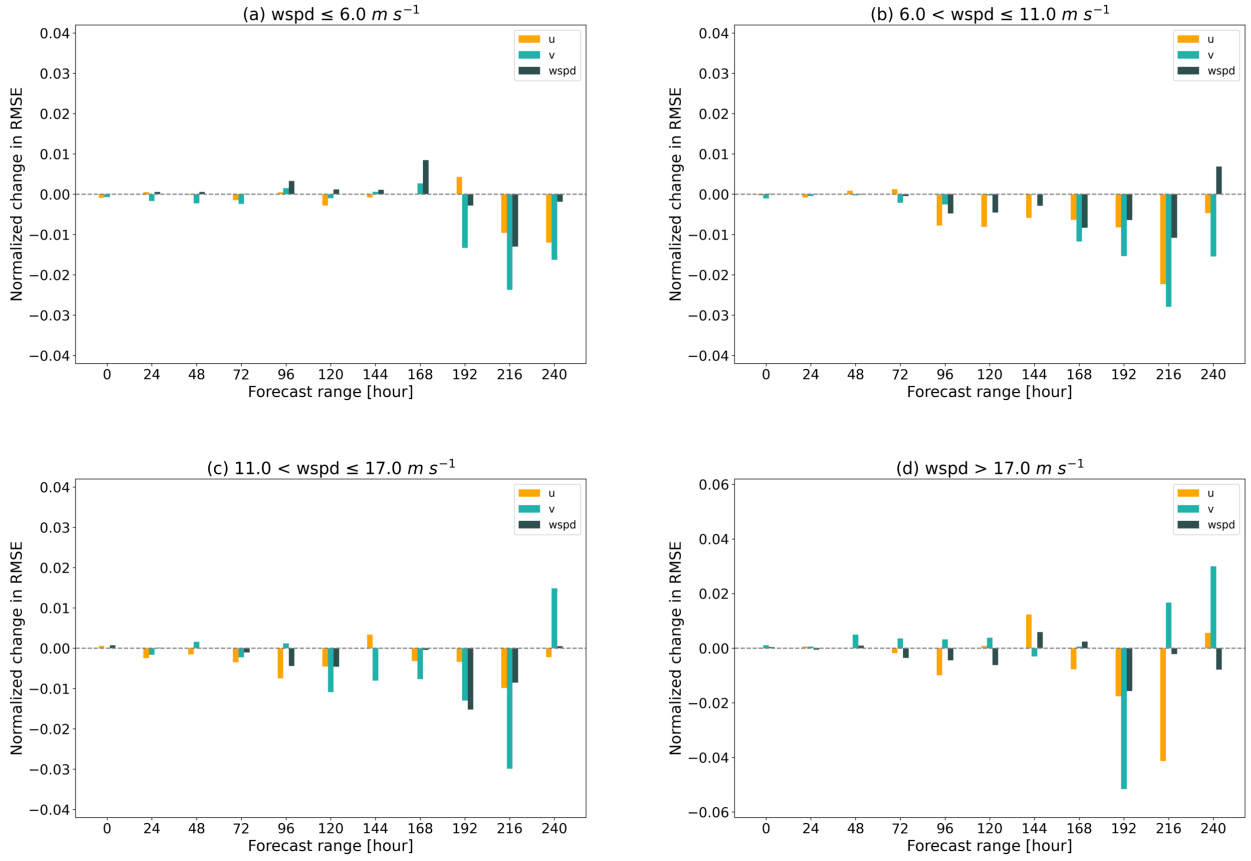

Figure 9: Same to Fig.8 but for different wind speed ranges.

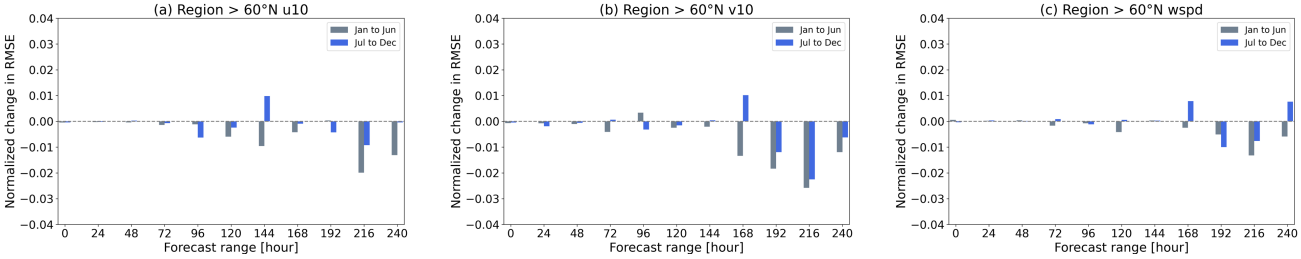

Figure 10: Normalized change in RMSE of u, v components and wind speed (wspd) as a function of forecast range during each half-year of 2020 for the region > 60° N based on the ECMWF OSE forecasts with and without Aeolus and weather station data.

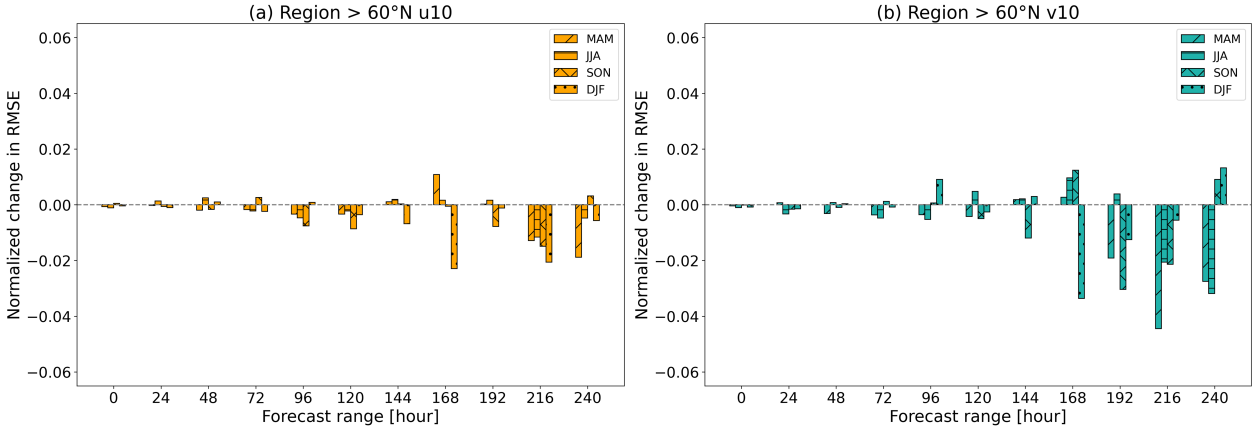

Figure 11: Seasonal normalized change in RMSE of u and v components as a function of forecast range for the region > 60° N for the year 2020 based on the ECMWF OSE forecasts with and without Aeolus and weather station data. MAM: March, April, and May; JJA: June, July, and August; SON: September, October, and November; DJF: December, January, and February.

4.2.2 Triple collocation analysis

The results of triple collocation analysis for the region > 60° N are given in Fig.12, 13 and 14. With forecast extending, the error standard deviations of u and v components from OSEs increase gradually from ~ 0.2 m s^{-1} to ~ 2.5 m s^{-1}, but the values from the experiments with Aeolus are slightly smaller than the ones without Aeolus assimilation, particularly from T+192 h for both u and v components (Fig.12). The error standard deviations of in situ measurements also increase from ~2.0 m s^{-1} to ~ 3.5 m s^{-1} for both u and v components, while the common true variances decrease to below 2 m^2 s^{-2} (Fig.12).

With respect to the results for each half-year (Fig. 13), evident error reductions caused by Aeolus are found at more forecast steps during the first half-year, with forecast improvement from T+120 h for the u component and T+168 h for the v component. In terms of the seasonal variation (Fig. 14), Aeolus tends to have more positive impacts on the forecast during boreal winter with smaller errors from T+144 h for the u component and from T+168 h for the v component. Significant error reductions are also found at T+216 h and T+240 h for the v component during boreal summer.

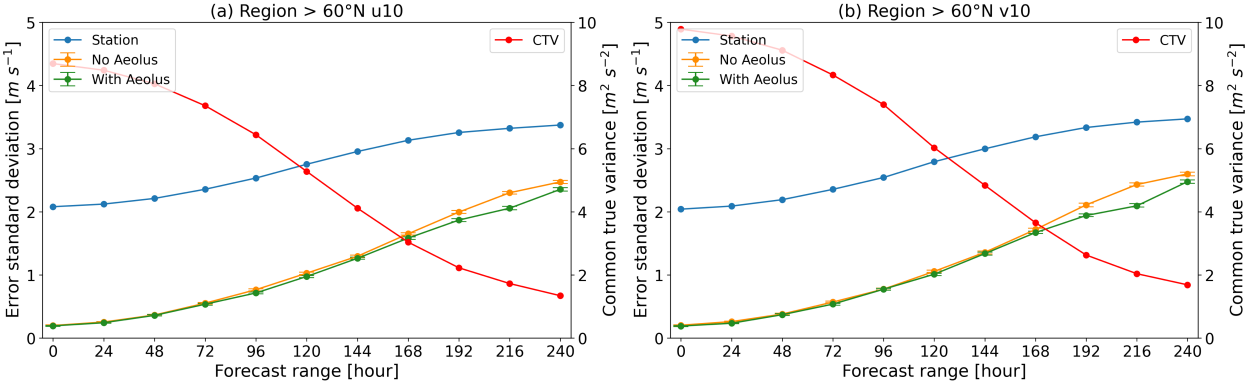

Figure 12: Error standard deviation and common true variance (CTV) of u and v components a function of forecast range for the region > 60° N for the year 2020 based on the ECMWF OSE forecast with and without Aeolus and weather station data.

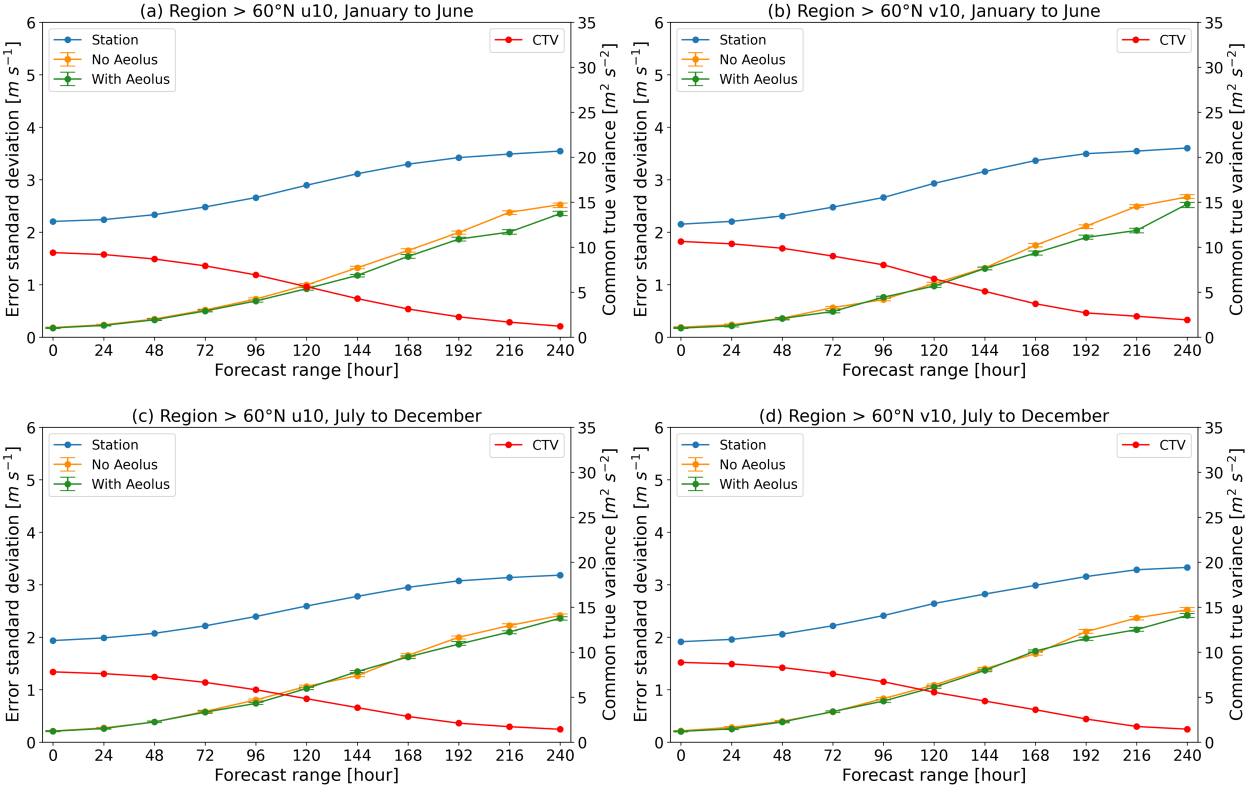

Figure 13: Same as Figure 10 but for the first (a and b) and the second half-year (c and d) of 2020.

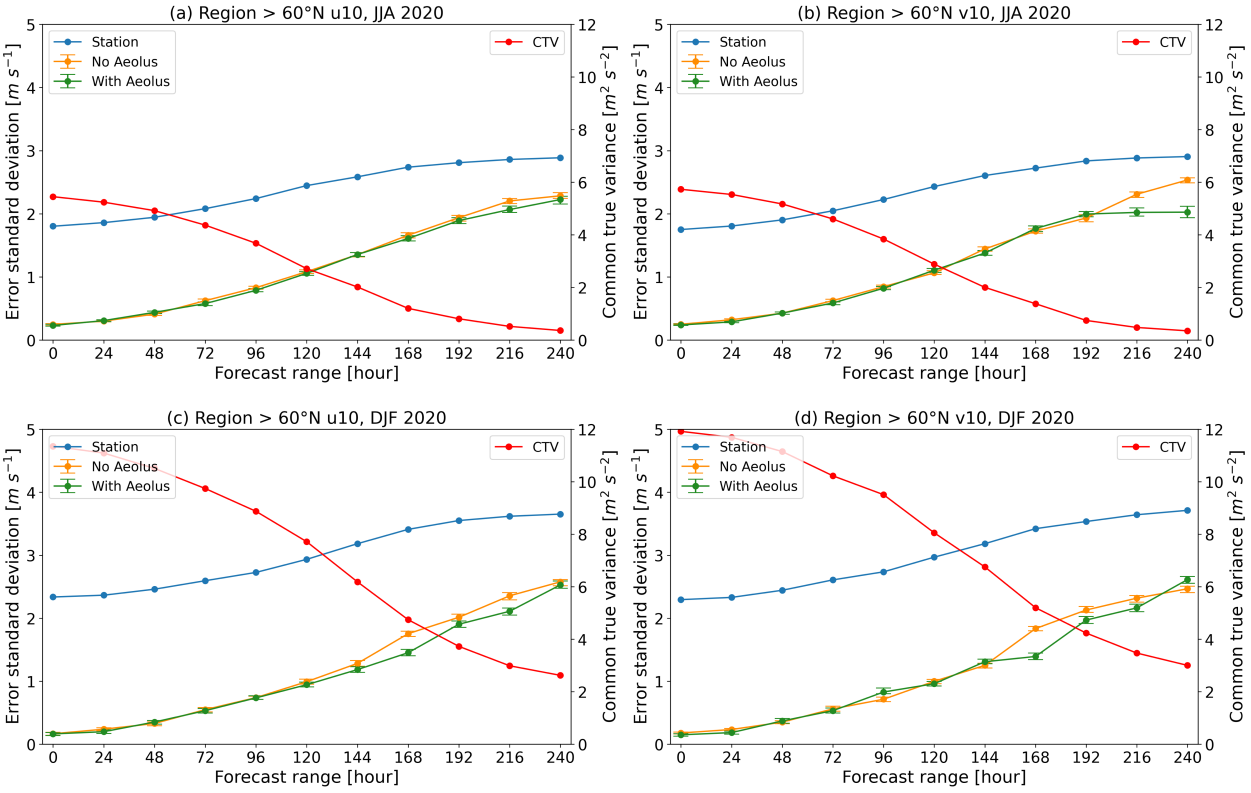

330 **Figure 14: Same as Fig. 10 but for boreal summer (a and b) and boreal winter (c and d), respectively.**

4.2.3 Correlations of datasets

Regarding the correlations for the region > 60° N, the wind components and wind speed between the two OSEs with and without Aeolus assimilation are well correlated as the forecast extends, with R-values greater than 0.90 until T+120 h (Fig.15 (a), (d) and (g)). Moreover, with the forecast extending, the R-values of the forecasts with Aeolus versus in situ
335 measurements are slightly larger than the ones without Aeolus data, which is in line with the inter-comparison analysis, suggesting a minimal improvement in wind forecast. However, different from the inter-comparison analysis, the R-value is

not sensitive to reflect which wind component can benefit more from Aeolus data assimilation.

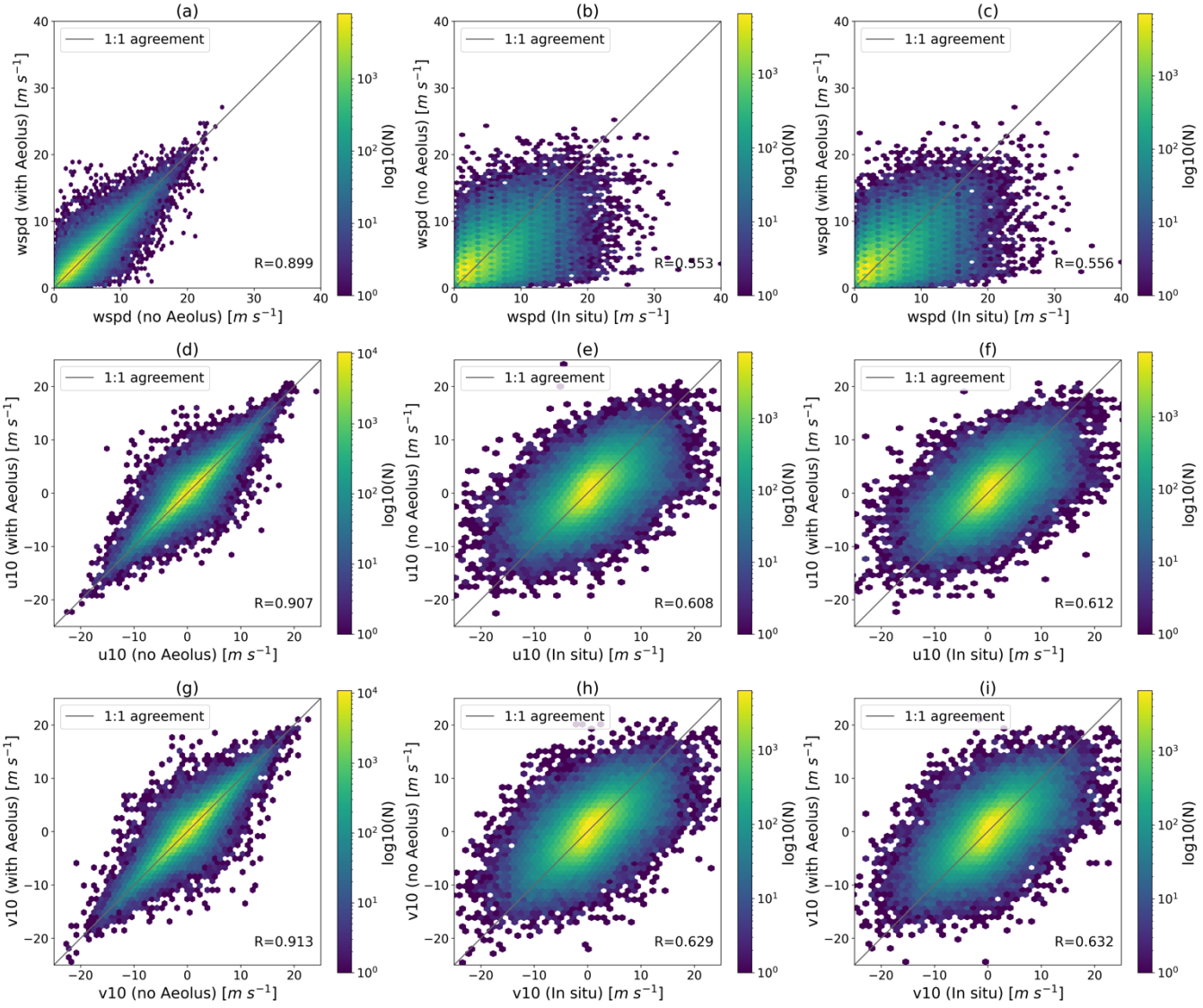

Figure 15: Hexagonal binning plots of u, v components and wind speed at T+120 h for the region > 60° N for the year 2020 based on the ECMWF OSE forecast with and without Aeolus and weather station data. The colour of each hexagon indicates the number of samples in it.

4.3 High-latitude region in the Southern Hemisphere (> 60° S)

4.3.1 Inter-comparison analysis

For the Southern Hemisphere, the impact of Aeolus on wind forecast is nearly neutral when considering the whole study period. The negative NCRMSEs were mainly found at T+96 h and +216 h, but the significant error reduction is only at T+216 h for wind speed forecast (Fig. 16). Regarding the results for two different half-years, more negative NCRMSEs of u component and wind speed were found within T+96 h and at T+216 h and T+240 h during the first half-year of 2020 (Fig. 17). With respect to the results for each season (Fig. 18), as forecast range extends, there are more negative NCRMSEs on u component than on v component although these exist randomly on any season.

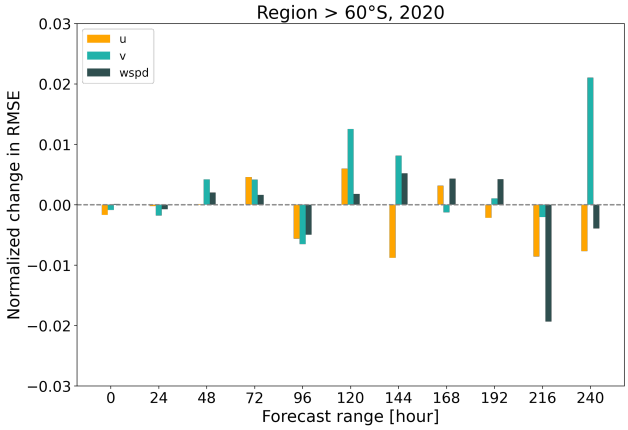

Figure 16: Normalized change in RMSE of u, v components and wind speed (wspd) as a function of forecast range for the region > 60° S for the year 2020 based on the ECMWF OSE forecasts with and without Aeolus and weather station data.

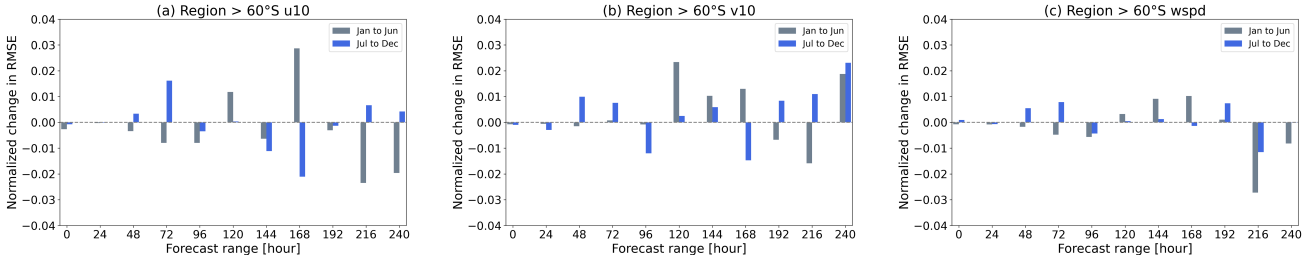

Figure 17: Normalized change in RMSE of u, v components as a function of forecast range for two different half years of 2020 for the region > 60° S based on the ECMWF OSE forecasts with and without Aeolus and weather station data.

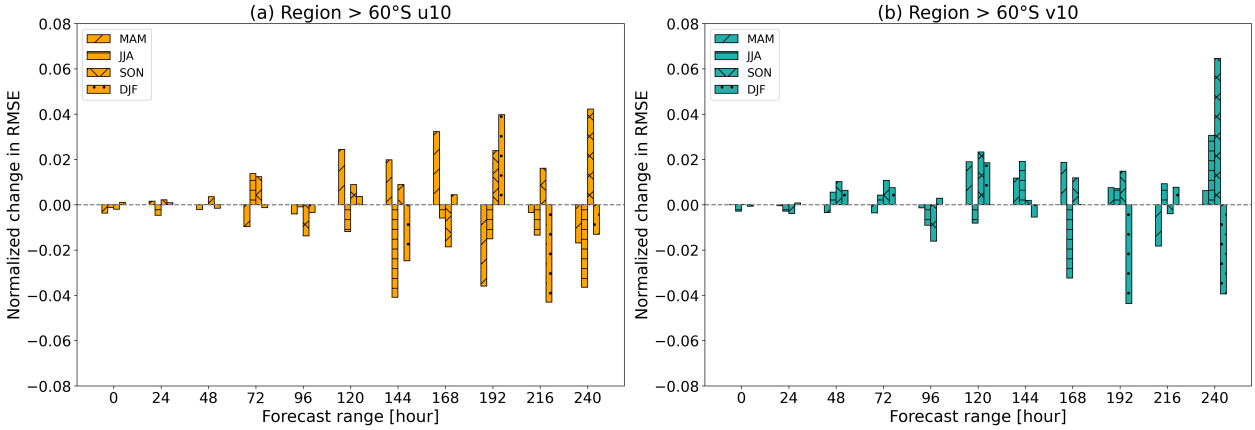

Figure 18: Seasonal normalized change in RMSE of u and v components as a function of forecast range for the region > 60° S for the year 2020 based on the ECMWF OSE forecasts with and without Aeolus and weather station data. MAM: March, April, and May; JJA: June, July, and August; SON: September, October, and November; DJF: December, January, and February.

4.3.2 Triple collocation analysis

The results of triple collocation analysis are consistent with the results from inter-comparison analysis. Almost no significant error reductions are found for both u and v components, and Aeolus even increases the forecast errors for the v component at some time steps (Fig. 19). The error standard deviations of the two OSEs increase from ~0.3 m s^{-1} at T+0 h to ~3.5 m s^{-1} and ~3.0 m s^{-1} at T+240 h for u and v components, respectively. In terms of the results for each half-year (Fig. 20), Aeolus has more positive impacts on the u component forecast with smaller errors at T+216 h and T+240 h during the first half-year of 2020. Regarding the results for seasons, Aeolus is likely to improve the forecasts on the u component from T+144 h during winter months (June, July and August), but the results have large uncertainties and need to be further confirmed (Fig. 21 (a)). For the v component, error reductions are mainly found at T+192 h and T+240 h during the summer months (December, January and February) (Fig. 21 (d)). In addition, errors of the OSEs and in situ measurements are found to be smaller during summer months than during winter months.

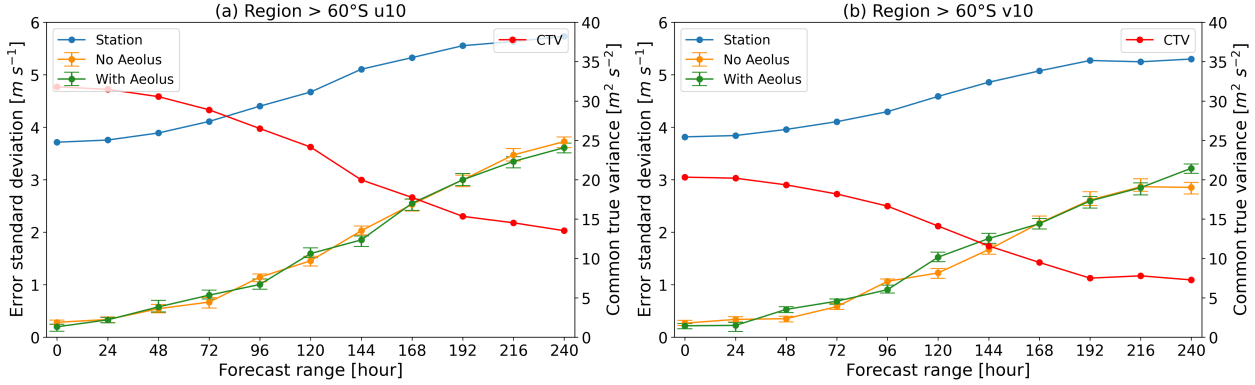

Figure 19: Error standard deviation and common true variance of u and v components as a function of forecast range for the region > 60° S for the year 2020 based on the ECMWF OSE forecasts with and without Aeolus and weather station data.

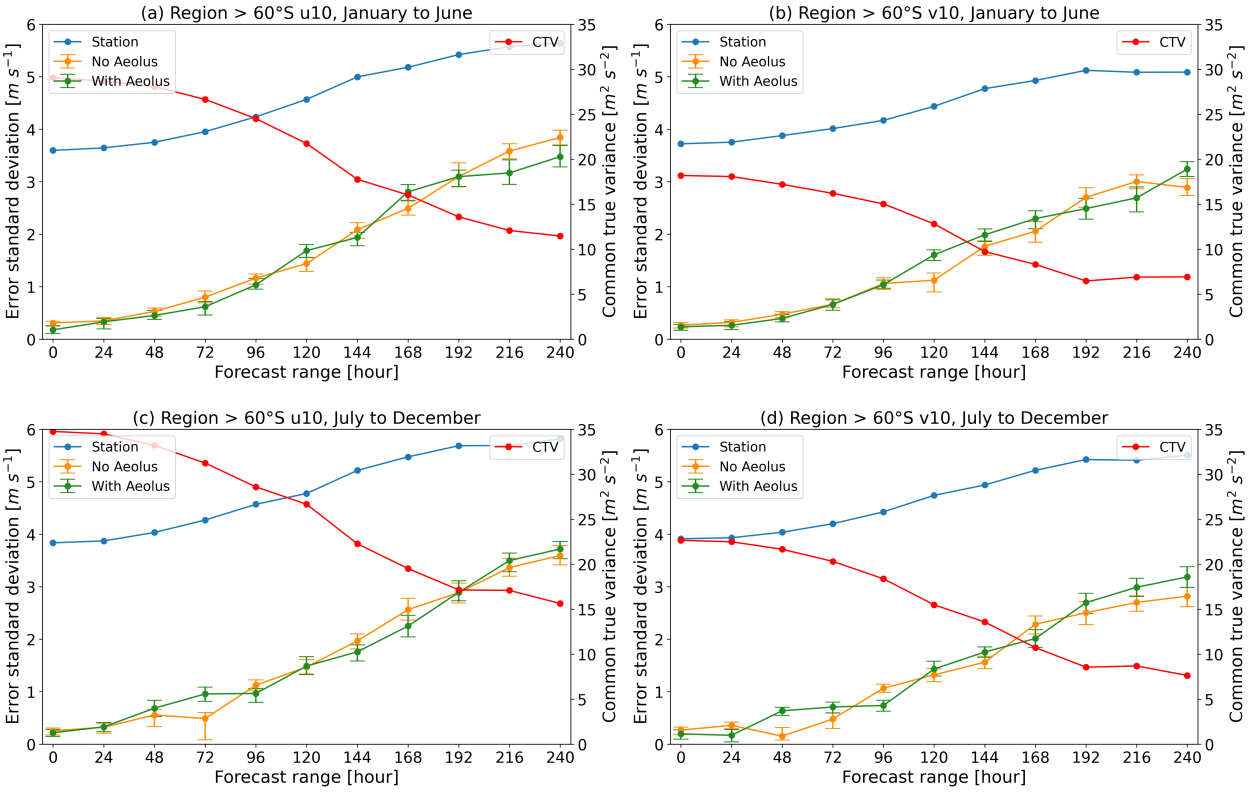

Figure 20: Same as Fig. 19 but for the first (a and b) and the second half-year (c and d) of 2020.

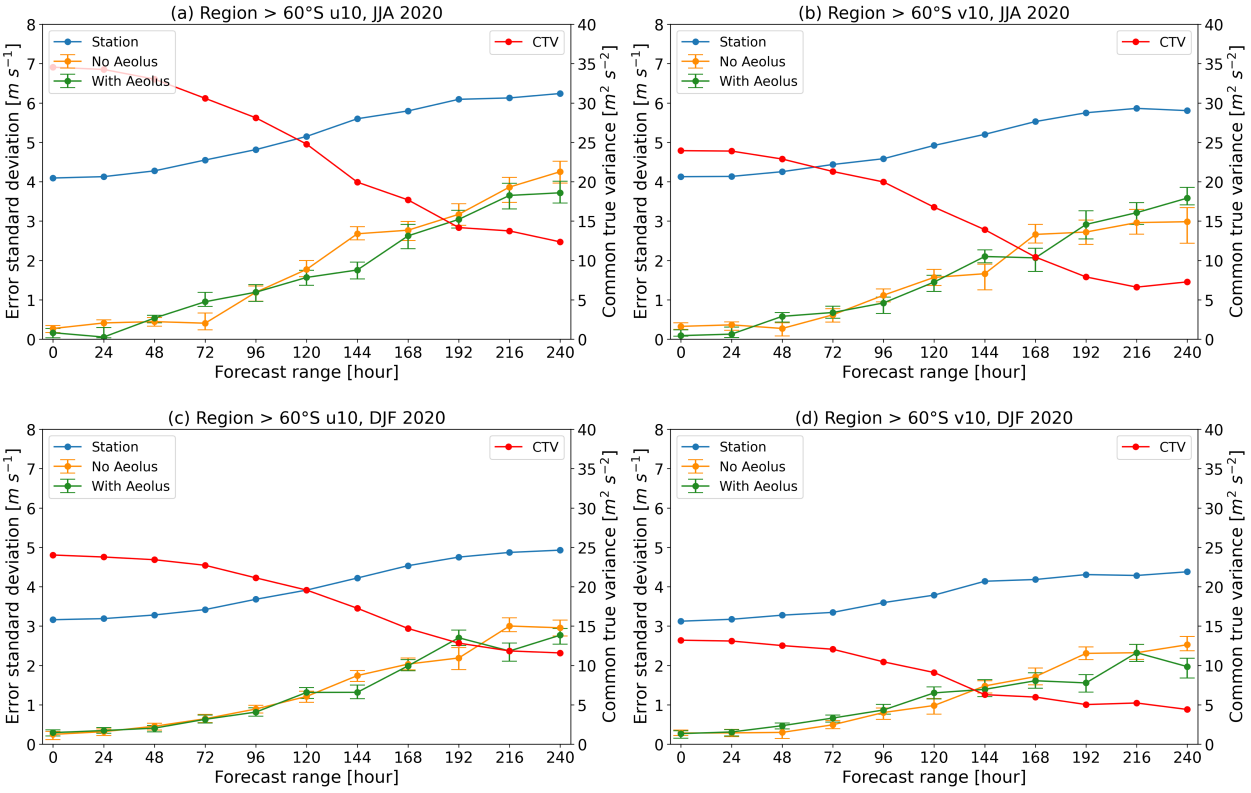

Figure 21: Same as Fig. 19 but for the winter months (June, July and August) and summer months (December, January, and February) in the Southern Hemisphere, respectively.

4.3.3 Correlations of datasets

About the correlations for the region > 60° S, the wind components and wind speed between the two OSEs show strong agreement as the forecast extends, with R values consistently greater than 0.89 up to T+120 h (Fig.22 (a), (d) and (g)). This pattern is comparable with the results for the region > 60° N, although the number of data samples is much lower in the region > 60° S. Moreover, the R-values of each two systems decrease gradually with forecast time, but the correlations for the u and v components are stronger than those for the wind speed for all forecast steps. In addition, the correlations between the OSEs and the in situ measurements are consistent with the inter-comparison results, with R-values of the forecast with Aeolus versus in situ data higher than the ones without Aeolus corresponding to the negative NCRMSEs.

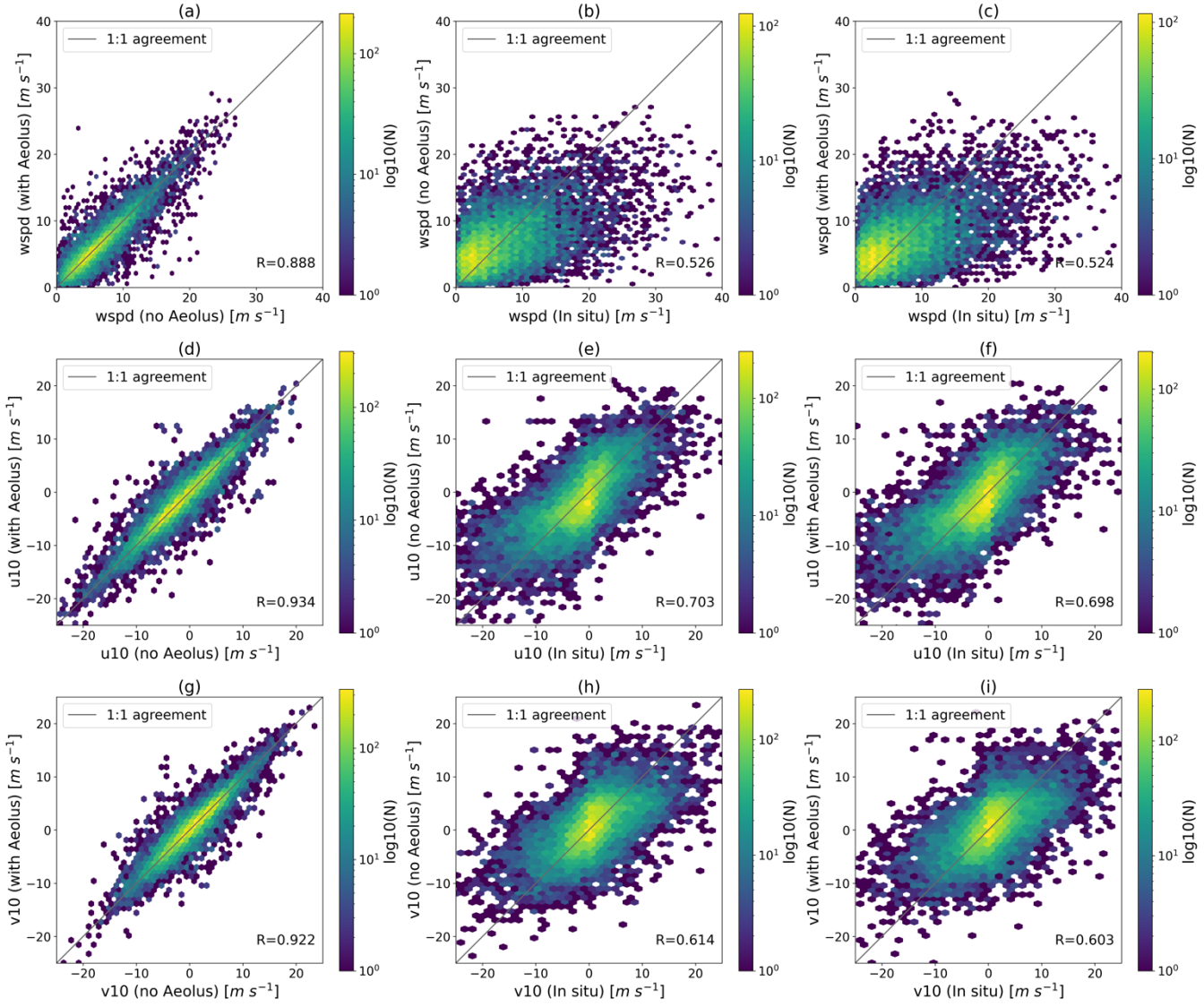

Figure 22: Scatter plots of u, v components and wind speed at +120 h forecast for the region > 60° S for the year 2020 based on the ECMWF OSE forecasts with and without Aeolus and weather station data. The colour of each hexagon indicates the number of samples in it.

5 Discussion

By taking in situ measurements as the reference, we evaluated the impact of Aeolus data assimilation on wind forecast at the near-surface level based on the ECMWF OSEs. According to the results of inter-comparison analyses for tropical oceans, the

impact of Aeolus on sea surface wind forecast is nearly neutral overall. However, negative NCRMSE values are observed across all three ocean basins at the T+48 h forecast step. Despite not being statistically significant, this result is consistent with the verifications based on the model analysis at ECMWF (Rennie and Isaksen, 2022), but further demonstration is required with more in situ measurements.

For the NH high-latitude region, Aeolus makes more positive impacts with forecast extending, which is possibly owing to the downward propagation of Aeolus increments to the surface since there are a limited number of low-level Aeolus winds inland assimilated into the model (Fig.1). Moreover, the greater positive impact is found for v component at many forecast steps. One possible reason is that at higher latitudes, Aeolus measurements are closer to meridional winds, thus leading to more impact on the v component. To assess the impact of Aeolus data quality on its contribution to wind forecast, we also divided the study period into two half-year periods. There are more evident error reductions during the first half-year than during the second half-year for the high-latitude region in the NH, which suggests that the increasing random errors of Aeolus due to signal loss may degrade its impacts on wind forecast at the surface level. With respect to the impact of different seasons, the results for the region > 60° N show that Aeolus tends to have a more positive impact on wind forecast during the winter months than during the summer months. This is partly attributed to the seasonal variation of solar background noise, which leads to larger random errors of Rayleigh-clear winds during summer months over polar regions and in the stratosphere (Reitebuch et al., 2022), thus resulting in larger forecast errors correspondingly. Another possible reason for the seasonal variation in error reduction is the different contributions of Aeolus data assimilation under different wind speed ranges. According to Fig.9, more error reductions are found when wind speeds are greater than 6 m s^{-1} for the region > 60° N. Thus, during the stormy season, which is usually the wintertime for the high-latitude regions, there could be more evident error reductions.

Different from the results for the high-latitude region in the NH, Aeolus winds seem to have a limited impact on improving wind forecast for the region > 60° S. This may be due to the poor spatial coverage of weather stations in Antarctica. Apart from this, the model may have a different performance when apply to the region > 60° S due to the ice sheet and mountainous terrain, which could impair the contribution of Aeolus.

In this study, the normalized change in the RMSEs between the control experiment and the experiment with Aeolus are not statistically significant at a significance level of 0.05 for many cases and forecast steps. We consider this in part to be due to the limited number of buoys and weather stations distributed over the study regions. Another possible reason could be the representativeness of the point-based measurements compared to the coarse model resolution, which makes the errors between in situ measurements and model outputs large and random.

The results from triple collocation analysis are consistent with the results from the inter-comparison analysis, with error standard deviations of forecast with Aeolus lower than the ones without Aeolus corresponding to the negative NCRMSEs and indicating a positive impact from the Aeolus. For all cases, the forecast errors are always smaller than the in situ measurement errors, especially for the short-term forecast since the result of triple collocation is with respect to the coarsest system (Vogelzang and Stoffelen, 2012), that is the ECMWF model resolution in this study. The effective resolution of the model is about 8 times of the grid size (Abdalla et al., 2013), so the effective resolution of the OSEs is about 144 km, which means the model can capture the large-scale signal of the atmosphere but lose small details, so the errors from the two OSEs are small. For the in situ measurements, such as buoys or weather stations which can detect the small-scale signal of the atmosphere, the large random errors are primarily caused by the temporal and spatial representation errors resulting from the collocation and the coarse model effective resolution. Another possible reason for the small forecast errors is that the wind forecasts for the first few days may not be fully independent of each other due to the limited number of Aeolus low-level winds assimilated into the model, which leads to $\langle e_2 e_3 \rangle \neq 0$. According to the Eq.(5)-(7), the error standard deviations for the OSEs may be underestimated, while those for the in situ measurements may be slightly overestimated. In addition, the error standard deviations of in situ measurements are found to increase with forecast steps. This is partly because as the forecasts extend in time and become noisier, the common true variances decrease as both the experiments with Aeolus and no Aeolus winds are unable to capture the smaller scale signals. Hence, the true small-scale signals measured by buoys or weather stations will go into the in situ noise (Ad Stoffelen, personal communication, 2022). This is why the in situ errors also grow with forecast time.

6 Conclusions

With the help of in situ measurements, the contribution of Aeolus wind assimilation to near-surface wind forecast was assessed for tropical oceans (between 30° N and 30° S) and high-latitude regions (> 60° N and > 60° S) through both inter-comparison analysis and triple collocation analysis. The wind predictions come from the high-resolution $T_{co}639$ OSEs with the ECMWF model.

The results indicate that Aeolus wind assimilation has limited impact on the sea surface wind forecasts for the tropical oceans, however, which requires further demonstration with more data samples. For the high-latitude region in the NH, error reductions are observed for many forecast steps, and this positive impact becomes more evident with forecast extending. Moreover, more error reductions are found during the first half-year of 2020 and during the winter months owing to the better behaviour of the Aeolus and its greater contribution to the moderate-to-strong wind forecasts. In addition, the v wind component is likely to benefit more from Aeolus data assimilation than the u component for the region > 60° N. Unlike the NH, the contribution of Aeolus to the region > 30° S is not obvious, and further investigation with more in situ measurements is required. The research findings from TC are consistent with the results from the inter-comparison analyses,

with an error standard deviation from the experiment with Aeolus data assimilation lower than the one without Aeolus corresponding to the negative NCRMSE, indicating a positive impact from Aeolus. The results from the TC method also suggest that the winds from the two OSEs are more precise than the in situ measurements in representing model scales.

Notwithstanding the limited spatial coverage of the reference data, the research findings of this study provide information on the role of Aeolus data assimilation with the ECMWF model in near-surface wind forecasts over the tropical ocean and the high-latitude regions.

Appendix A

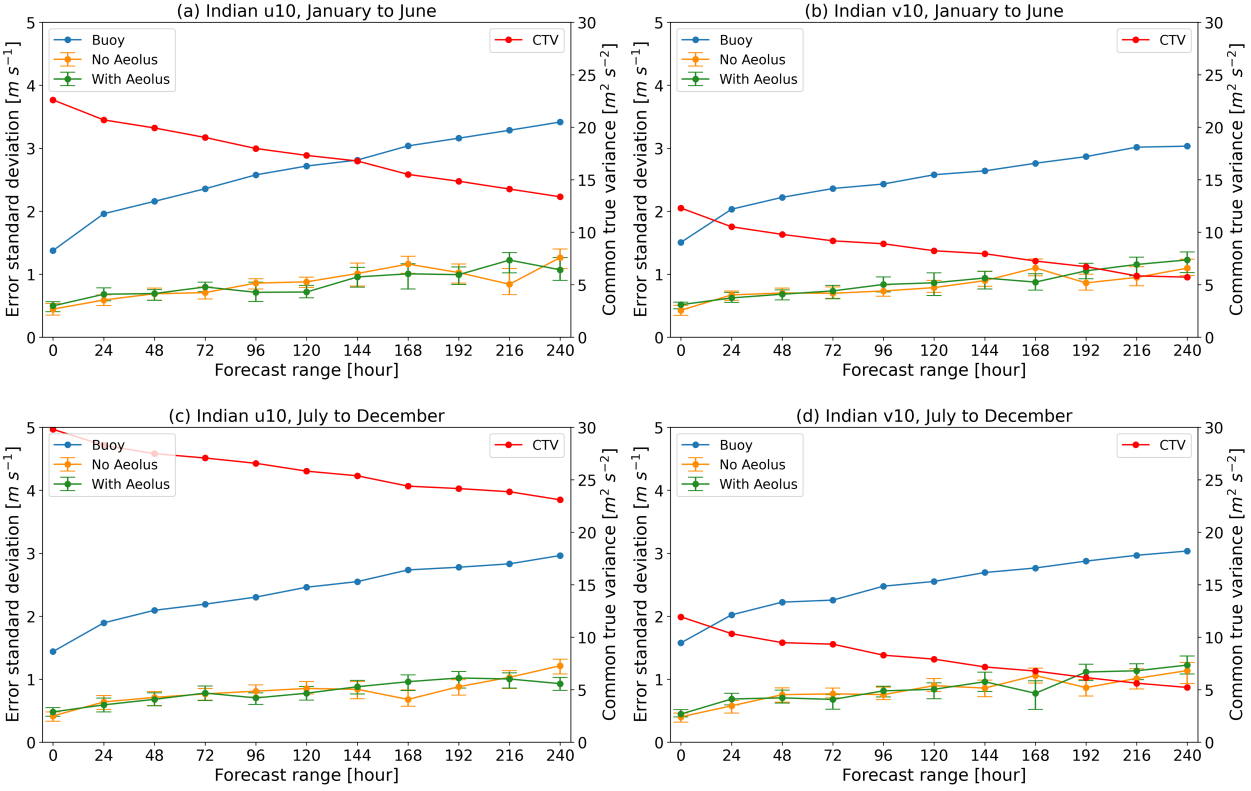

Figure A1: Error standard deviations and common true variances of u and v components as a function of forecast range for the tropical Indian Ocean for the two half-year periods of 2020. January to June: (a) and (b); July to December: (c) and (d).

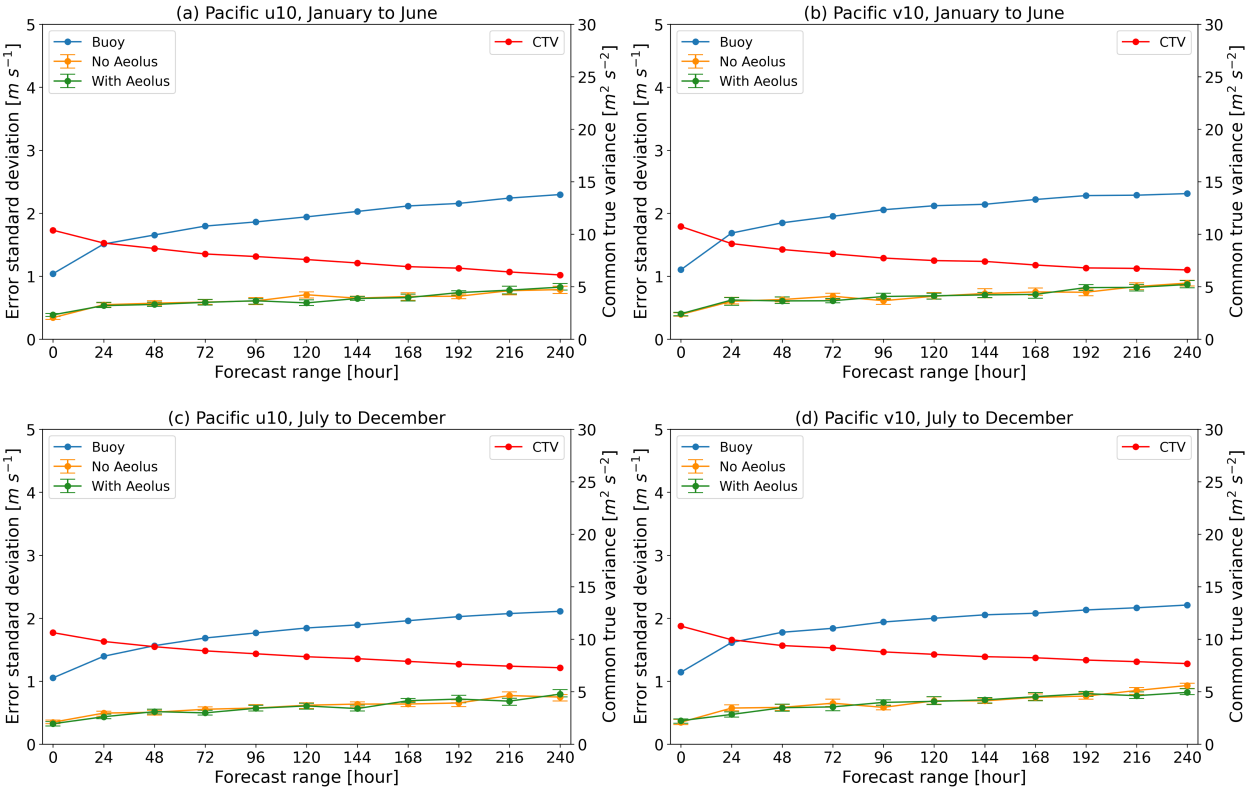

Figure A2: Same as Fig. A1 but for the tropical Pacific Ocean.

Data availability. The OSEs were conducted by Michael Rennie and Lars Isaksen from the ECMWF, and the u and v wind components were extracted from MARS (https://apps.ecmwf.int/mars-catalogue/, last access: 28 July 2022, ECMWF). The buoy measurements were obtained from Global Tropical Moored Buoy Array (https://www.pmel.noaa.gov/tao/drupal/disdel/, last access: 04 August 2022, National Oceanic and Atmospheric Administration Pacific Marine Environmental Laboratory). Wind information at weather stations is accessed via Global Hourly - Integrated Surface Database (https://www.ncei.noaa.gov/products/land-based-station/integrated-surface-database#:~:text=Global%20Climate%20Station%20Summaries%20Summaries%20are%20simple%20indicators,or%20longer%20time%20periods%20or%20for%20customized%20periods., last access: 11 August 2022, National Centers for Environmental Information).

Author contributions. HZ obtained the data, performed the data analysis, and drafted the manuscript. CH helped in interpreting the research findings. HZ revised the manuscript critically.

Competing interests. The authors declare that they have no conflict of interest.

Acknowledgement. This study is a part of PhD project Aeolus satellite lidar for wind mapping, a sub-project of the LIdar Knowledge Europe (LIKE) Innovative Training Network (ITN) Marie Skłodowska-Curie Actions funded by European Union Horizon 2020 (Grant number: 858358). We would like to thank the Royal Netherlands Meteorological Institute (KNMI) for being the secondment host institution. Our special appreciation goes to Ad Stoffelen from KNMI who gave us the idea to conduct this study and to Gert-Jan Marseille from KNMI for his assistance with OSE data retrieval. We would also like to show our gratitude to Michael Rennie and Lars Isaksen from the ECMWF for conducting the OSEs and providing the data for analysis. We thank the National Oceanic and Atmospheric Administration Pacific Marine Environmental Laboratory for buoy data and the National Centers for Environmental Information for wind measurements at weather stations.

Financial support. This research is a part of the PhD project Aeolus Satellite Lidar for Wind Mapping, a sub-project of the Innovation Training Network Marie Skłodowska-Curie Actions: Lidar Knowledge Europe (LIKE) supported by the European Union Horizon 2020 (Grant number: 858358).

References

Abdalla, S., Isaksen, L., Janssen, P. A. E. M., and Wedi, N.: Effective spectral resolution of ECMWF atmospheric forecast models, ECMWF, Newsletter Number 137, 19–22, doi:10.21957/rue4o7ac, 2013.

Andersson, E., Dabas, A., Endemann, M., Ingmann, P., Källén, E., Offiler, D., and Stoffelen, A.: ADM-Aeolus Science Report, SP-1311, ESA, 121 pp., https://esamultimedia.esa.int/multimedia/publications/SP-1311/SP-1311.pdf (last access: 2 September 2022), 2008.

Banyard, T. P., Wright, C. J., Hindley, N. P., Halloran, G., Krisch, I., Kaifler, B., and Hoffmann, L.: Atmospheric Gravity Waves in Aeolus Wind Lidar Observations, Geophys. Res. Lett., 48, e2021GL092756, https://doi.org/10.1029/2021GL092756, 2021.

Belova, E., Kirkwood, S., Voelger, P., Chatterjee, S., Satheesan, K., Hagelin, S., Lindskog, M., and Körnich, H.: Validation of Aeolus winds using ground-based radars in Antarctica and in northern Sweden, Atmos. Meas. Tech., 14, 5415–5428, https://doi.org/10.5194/amt-14-5415-2021, 2021.

Bidlot, J.-R., Holmes, D. J., Wittmann, P. A., Lalbeharry, R., and Chen, H. S.: Intercomparison of the Performance of Operational Ocean Wave Forecasting Systems with Buoy Data, Wea. Forecasting, 17, 287–310, https://doi.org/10.1175/1520-0434(2002)017<0287:IOTPOO>2.0.CO;2, 2002.

Caires, S. and Sterl, A.: Validation of ocean wind and wave data using triple collocation, J. Geophys. Res., 108, 3098, https://doi.org/10.1029/2002JC001491, 2003.

Cossu, F., Portabella, M., Lin, W., Stoffelen, A., Vogelzang, J., Marseille, G.-J., and de Haan, S.: Characterization of Aeolus Measurement Errors by Triple Collocation Analysis Over Western Europe, in: IGARSS 2022 - 2022 IEEE International Geoscience and Remote Sensing Symposium, IGARSS 2022 - 2022 IEEE International Geoscience and Remote Sensing Symposium, Kuala Lumpur, Malaysia, 17-22 July 2022, 6494–6497, https://doi.org/10.1109/IGARSS46834.2022.9883249, 2022.

Cress, A., Martin, A., Born, M., and Weismann, M.: Impact of Aeolus HLOS winds in the global NWP System of DWD, Towards an operational Doppler Wind Lidar Programm, Darmstadt, Germany, 8-9 September 2022, https://www.eventsforce.net/eumetsat/frontend/reg/tAgendaWebsite.csp?pageID=15588&ef_sel_menu=247&eventID=38&mode= , 2022.

Data Innovation and Science Cluster (DISC): Summary of Quality of Aeolus Data Products from 1st Reprocessing Campaign covering June to December 2019, ESA, https://earth.esa.int/eogateway/documents/20142/0/Aeolus-Summary-Reprocessing-1-DISC.pdf (last access: 02 November 2022), 2020.

ECMWF: Fact sheet: Earth system data assimilation, ECMWF, https://www.ecmwf.int/sites/default/files/medialibrary/2020-05/ecmwf-fact-sheet-data-assimilation.pdf (last access: 10 November 2022), 2020.

ECMWF: ECMWF Research Experiments (RD), ECMWF [data set], https://www.ecmwf.int/en/forecasts/dataset/ecmwf-research-experiments (last access: 20 July 2022), 2022.

Forsythe, M. and Halloran, G.: Impact of Aeolus Doppler Wind Lidar at the UK Met Office, Towards an operational Doppler Wind Lidar Programm, Darmstadt, Germany, 8-9 September 2022, https://www.eventsforce.net/eumetsat/frontend/reg/tAgendaWebsite.csp?pageID=15588&ef_sel_menu=247&eventID=38&mode= , 2022.

Garrett, K., Liu, H., Ide, K., Hoffman, R. N., and Lukens, K. E.: Optimization and impact assessment of Aeolus HLOS wind assimilation in NOAA's global forecast system, Quart. J. Royal. Meteoro. Soc., 148, 2703–2716, https://doi.org/10.1002/qj.4331, 2022.

Hagelin, S., Azad, R., Lindskog, M., Schyberg, H., and Körnich, H.: Evaluating the use of Aeolus satellite observations in the regional numerical weather prediction (NWP) model Harmonie–Arome, Atmos. Meas. Tech., 14, 5925–5938, https://doi.org/10.5194/amt-14-5925-2021, 2021.

Iwai, H., Aoki, M., Oshiro, M., and Ishii, S.: Validation of Aeolus Level 2B wind products using wind profilers, ground-based Doppler wind lidars, and radiosondes in Japan, Atmos. Meas. Tech., 14, 7255–7275, https://doi.org/10.5194/amt-14-7255-2021, 2021.

King, G. P., Portabella, M., Lin, W., and Stoffelen, A.: Correlating extremes in wind divergence with extremes in rain over the Tropical Atlantic, https://mdc.coaps.fsu.edu/scatterometry/meeting/docs/2022/King-IOVWST-2022.pdf (last access: 06 March 2022), 2023.

Laroche, S. and St-James, J.: Impact of the Aeolus Level-2B horizontal line-of-sight winds in the Environment and Climate Change Canada global forecast system, Quart. J. Royal. Meteoro. Soc., 148, 2047–2062, https://doi.org/10.1002/qj.4300, 2022.

Met Office: Beaufort wind force scale, https://www.metoffice.gov.uk/weather/guides/coast-and-sea/beaufort-scale, last access: 24 February 2023.

Mile, M., Azad, R., and Marseille, G.: Assimilation of Aeolus Rayleigh-Clear Winds Using a Footprint Operator in AROME-Arctic Mesoscale Model, Geophysical Research Letters, 49, 1–11, https://doi.org/10.1029/2021GL097615, 2022.

National Centers for Environmental Information (NCEI): Global Hourly - Integrated Surface Database (ISD), NCEI [data set], National Oceanic and Atmospheric Administration, https://www.ncei.noaa.gov/products/land-based-station/integrated-surface-database#:~:text=Global%20Climate%20Station%20Summaries%20Summaries%20are%20simple%20indicators,or%20longer%20time%20periods%20or%20for%20customized%20periods. (last access: 11 August 2022), n.d.

Parrington, M., Rennie, M., Inness, A., and Duncan, D.: Monitoring the atmospheric impacts of the Hunga-Tonga eruption, ECMWF, https://www.ecmwf.int/en/newsletter/171/news/monitoring-atmospheric-impacts-hunga-tonga-eruption, last access: 2 November 2022, 2022.

Pacific Marine Environmental Laboratory (PMEL): Global Tropical Moored Buoy Array, PMEL [Data set], National Oceanic and Atmospheric Administration, https://www.pmel.noaa.gov/gtmba/ (last access: 03 August 2022), n.d.

Pourret, V., Šavli, M., Mahfouf, J., Raspaud, D., Doerenbecher, A., Bénichou, H., and Payan, C.: Operational assimilation of Aeolus winds in the Météo-France global NWP model ARPEGE, Quart. J. Royal. Meteoro. Soc., 148, 2652–2671, https://doi.org/10.1002/qj.4329, 2022.

Reitebuch, O., Krisch, I., Lemmerz, C., Lux, O., Marksteiner, U., Masoumzadeh, N., Weiler, F., Witschas, B., Filomarino, V. C., Meringer, M., Schmidt, K., Huber, D., Nikolaus, I., Fabre, F., Vaughan, M., Reissig, K., Dabas, A., Flament, T., Lacour, A., Mahfouf, J.-F., Seck, I., Trapon, D., Abdalla, S., Isaksen, L., Rennie, M., Benedetti, A., McLean, W., Henry, K., Donovan, D., de Kloe, J., Marseille, G.-J., Stoffelen, A., Wang, P., van Zadelhoff, G.-J., Perron, G., Jupin-Langlois, S., Pijnacker-Hordijk, B., Veneziani, M., Bucci, S., Gostinicchi, G., Di Ciolo, L., Bley, S., Geiss, A., Kanitz, T., Straume, A.-G., Wernham, D., Krisna, T., von Bismarck, J., Colangeli, G., Trivigno, V., Romanazzo, M., Aprile, S., and Parrinello, T.: Contributions from the DISC to accomplish the Aeolus mission objectives, Aeolus 3rd Anniversary Conference, Taormina, Italy, 23-27 March 2022, https://elib.dlr.de/186034/, 2022.

Rennie, M. and Isaksen, L.: The NWP impact of Aeolus Level-2B winds at ECMWF, ECMWF, 227 pp., https://confluence.ecmwf.int/display/AEOL/L2B+team+technical+reports+and+relevant+papers?preview=/46596815/288355970/AED-TN-ECMWF-NWP-025--20220810_v5.0.pdf (last access: 20 October 2022), 2022.

Rennie, M. P., Isaksen, L., Weiler, F., Kloe, J., Kanitz, T., and Reitebuch, O.: The impact of Aeolus wind retrievals on ECMWF global weather forecasts, Q. J. R. Meteorol. Soc., 147, 3555–3586, https://doi.org/10.1002/qj.4142, 2021.

Ribal, A. and Young, I. R.: Global Calibration and Error Estimation of Altimeter, Scatterometer, and Radiometer Wind Speed Using Triple Collocation, Remote Sens., 12, 1997, https://doi.org/10.3390/rs12121997, 2020.

Sandu, I., Bechtold, P., Nuijens, L., Beljaars, A., and Brown, A.: On the causes of systematic forecast biases in near-surface wind direction over the oceans, ECMWF, 21 pp., https://www.ecmwf.int/sites/default/files/elibrary/2020/19545-causes-systematic-forecast-biases-near-surface-wind-direction-over-oceans.pdf (last access: 22 February 2023), 2020.

Stoffelen, A.: Toward the true near-surface wind speed: Error modeling and calibration using triple collocation, J. Geophys. Res., 103, 7755–7766, https://doi.org/10.1029/97JC03180, 1998.

Straume-Lindner, A. G., Parrinello, T., Von Bismarck, J., Bley, S., Wernham, D., Kanitz, T., Alvarez, E., Fischey, P., De Laurentis, M., Fehr, T., Ehlers, F., Duc Tran, V., Krisch, I., Reitebuch, O., and Renni, M.: ESA'S Wind Mission Aeolus - Overview, Status and Outlook, in: 2021 IEEE International Geoscience and Remote Sensing Symposium IGARSS, IGARSS 2021 - 2021 IEEE International Geoscience and Remote Sensing Symposium, Brussels, Belgium, 12-16 July 2021, 755–758, https://doi.org/10.1109/IGARSS47720.2021.9554007, 2021.

Vogelzang, J. and Stoffelen, A.: Triple collocation, Royal Netherlands Meteorological Institute, 22 pp., https://cdn.knmi.nl/system/data_center_publications/files/000/068/914/original/triplecollocation_nwpsaf_tr_kn_021_v1.0.pdf?1495621500 (last access: 27 January 2022), 2012.

Vogelzang, J., Stoffelen, A., Verhoef, A., and Figa-Saldaña, J.: On the quality of high-resolution scatterometer winds, J. Geophys. Res., 116, C10033, https://doi.org/10.1029/2010JC006640, 2011.

Witschas, B., Lemmerz, C., Geiß, A., Lux, O., Marksteiner, U., Rahm, S., Reitebuch, O., Schäfler, A., and Weiler, F.: Validation of the Aeolus L2B wind product with airborne wind lidar measurements in the polar North Atlantic region and in the tropics, Atmos. Meas. Tech., 15, 7049–7070, https://doi.org/10.5194/amt-15-7049-2022, 2022.

Zuo, H., Hasager, C. B., Karagali, I., Stoffelen, A., Marseille, G.-J., and de Kloe, J.: Evaluation of Aeolus L2B wind product with wind profiling radar measurements and numerical weather prediction model equivalents over Australia, Atmos. Meas. Tech., 15, 4107–4124, https://doi.org/10.5194/amt-15-4107-2022, 2022.